

4

AFGL-TR-89-0072

Collision Dynamics and Transition
Probabilities for Vibrationally
Excited OH

Richard A. Copeland

SRI International
333 Ravenswood Avenue
Menlo Park, CA 94025

January 1989

Final Report
Period Covered June 1, 1987 to December 31, 1988

Approved for public release;
distribution unlimited

DTIC
ELECTE
MAY 03 1989
S E D

AIR FORCE GEOPHYSICS LABORATORY
AIR FORCE SYSTEMS COMMAND
UNITED STATES AIR FORCE
HANSCOM AIR FORCE BASE, MASSACHUSETTS 01731-5000


AD-A207 856

089 00 088

"This technical report has been reviewed and is approved for publication"

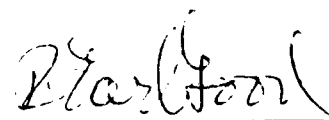

(Signature)

Steven M. Miller
Contract Manager


(Signature)

George A. Vanasse
Branch Chief

FOR THE COMMANDER


(Signature)
R. EARL GOOD
Director

This report has been reviewed by the ESD Public Affairs Office (PA) and is releasable to the National Technical Information Service (NTIS).

Qualified requestors may obtain additional copies from the Defense Technical Information Center. All others should apply to the National Technical Information Service.

If your address has changed, or if you wish to be removed from the mailing list, or if the addressee is no longer employed by your organization, please notify AFGL/DAA, Hanscom AFB, MA 01731. This will assist us in maintaining a current mailing list.

Do not return copies of this report unless contractual obligations or notices on a specific document requires that it be returned.

REPORT DOCUMENTATION PAGE

Form Approved
OMB No. 0704-0188

1a. REPORT SECURITY CLASSIFICATION Unclassified			1b. RESTRICTIVE MARKINGS		
2a. SECURITY CLASSIFICATION AUTHORITY			3. DISTRIBUTION/AVAILABILITY OF REPORT Approved for public release; distribution unlimited		
2b. DECLASSIFICATION/DOWNGRADING SCHEDULE					
4. PERFORMING ORGANIZATION REPORT NUMBER(S)			5. MONITORING ORGANIZATION REPORT NUMBER(S) AFGL-TR-89-0072		
6a. NAME OF PERFORMING ORGANIZATION SRI International	6b. OFFICE SYMBOL (if applicable)	7a. NAME OF MONITORING ORGANIZATION Air Force Geophysics Laboratory			
6c. ADDRESS (City, State, and ZIP Code) 333 Ravenswood Avenue Menlo Park, CA 94025		7b. ADDRESS (City, State, and ZIP Code) Hanscom AFB Massachusetts 01731-5000			
8a. NAME OF FUNDING/SPONSORING ORGANIZATION	8b. OFFICE SYMBOL (if applicable)	9. PROCUREMENT INSTRUMENT IDENTIFICATION NUMBER F19628-87-K-0043			
8c. ADDRESS (City, State, and ZIP Code)		10. SOURCE OF FUNDING NUMBERS			
		PROGRAM ELEMENT NO. 61102F	PROJECT NO. 2310	TASK NO. G4	WORK UNIT ACCESSION NO. BT
11. TITLE (Include Security Classification) Collision Dynamics and Transition Probabilities for Vibrationally Excited OH					
12. PERSONAL AUTHOR(S) Richard A. Copeland					
13a. TYPE OF REPORT Final Report	13b. TIME COVERED FROM 6/1/87 TO 12/31/88	14. DATE OF REPORT (Year, Month, Day) 1989 January	15. PAGE COUNT 60		
16. SUPPLEMENTARY NOTATION					
17. COSATI CODES			18. SUBJECT TERMS (Continue on reverse if necessary and identify by block number)		
FIELD	GROUP	SUB-GROUP			
			Collision Dynamics, OH, Transition Probabilities, Rotational Energy Transfer, Laser-Induced Fluorescence, Meinel Bands, Vibrational Energy Transfer, Hydroxyl Radical.		
19. ABSTRACT (Continue on reverse if necessary and identify by block number)					
<p>Vibrationally excited OH is a significant source of infrared emission in the upper atmosphere. Modeling the nonequilibrium processes responsible for the emission between vibrational levels in the ground state (called the Meinel bands) requires values for absolute transition probabilities and vibrational energy transfer rate constants for OH. However, the accuracy of currently available information is questionable. Most experimental studies have used the Meinel band emission itself to measure these quantities, with limited success. This report describes the development of a new laser-induced fluorescence method for detecting high-lying vibrational levels of OH. This sensitive and selective method employing excitation via the $B^2\Sigma^+ - X^2\Pi_i$ electronic transition can be used to study vibrational energy transfer rate constants and mechanisms in the high vibrational levels of ground-state OH. Experiments are described that test theoretical calculations of the relative magnitude of transitions from the B state to high vibrational levels of the A and X states and examine the applicability of B-X laser-induced fluorescence as a diagnostic method.</p>					
20. DISTRIBUTION/AVAILABILITY OF ABSTRACT <input checked="" type="checkbox"/> UNCLASSIFIED/UNLIMITED <input type="checkbox"/> SAME AS RPT. <input type="checkbox"/> DTIC USERS			21. ABSTRACT SECURITY CLASSIFICATION Unclassified		
22a. NAME OF RESPONSIBLE INDIVIDUAL Steven Miller			22b. TELEPHONE (Include Area Code)	22c. OFFICE SYMBOL AFGL/OPI	

CONTENTS

SUMMARY	ii
INTRODUCTION	1
BACKGROUND	2
Atmospheric Studies	2
Laboratory and Theoretical Studies	2
EXPERIMENTAL APPROACH	4
Production of OH*	4
Detection of OH*	6
RESULTS	11
Relative Vibrational Band Transition Probabilities	11
Fluorescence Lifetimes of B State	12
Advantages and Disadvantages of B-X LIF	23
CONCLUSIONS	24
MANUSCRIPTS, PRESENTATIONS, AND PERSONNEL	25
REFERENCES	26
APPENDICES	
A LASER-INDUCED FLUORESCENCE OF THE $B^2\Sigma^+-X^2\Pi_i$ SYSTEM OF OH: DETECTION OF $v = 8$ AND 9	A-1
B LASER-INDUCED FLUORESCENCE OF THE $B^2\Sigma^+-X^2\Pi_i$ SYSTEM OF OH	B-1



Accession For	
NTIS GRA&I	<input checked="" type="checkbox"/>
DTIC TAB	<input type="checkbox"/>
Unannounced	<input type="checkbox"/>
Justification	
By _____	
Distribution/	
Availability Codes	
Dist	Avail and/or Special
A-1	

FIGURES

1	Chemiluminescence downstream of an oxygen discharge with added propylene	5
2	OH* chemiluminescence from the reaction of H + O ₃ in a discharge flow cell	7
3	OH potential energy curves for the four lowest doublet states.....	8
4	Time evolution of the B-X LIF signal after excitation of two different rotational levels in OH (B ² Σ ⁺ , v' = 0).....	13
5	Plot of the decay constant for LIF after excitation of different rotational levels in OH (B ² Σ ⁺ , v' = 0, F ₁) versus the helium pressure.....	15
6	Plot of the decay constant versus rare gas pressure.....	18
7	Plot of the decay constant versus helium pressure after excitation of different fine-structured levels in OH(B ² Σ ⁺ , v' = 1, N' = 2).....	20

INTRODUCTION

Understanding the chemical and physical characteristics of the earth's atmosphere requires input from a variety of sources. Field measurements, theoretical calculations, atmospheric modeling, and laboratory studies all supply information to increase our knowledge of this complicated system. In this report, we describe laboratory measurements on vibrationally excited ground-state hydroxyl radical (OH^*) that will aid in the characterization of this important atmospheric species. Emission from OH^* is a significant component of the nightglow. Vibrational band transition probabilities and vibrational energy transfer (VET) rate constants are needed to model the emission and relate it to the underlying physical and chemical processes. The experiments described below are the first step in measuring the required input data, the development of sensitive and state-selective diagnostic methods for detection of OH^* .

The vibrational band transition probabilities and VET rate constants have been studied extensively; however, inconsistencies and disagreements abound. Both the importance to atmospheric phenomena and the earlier measurements of these values are described below. Rather than proceeding along the same experimental line as earlier studies, we chose to develop a new laser-induced fluorescence (LIF) diagnostic technique to apply to the OH system. Our experiments on $\text{B}^2\Sigma^+ - \text{X}^2\Pi_i$ LIF show that this new approach will prove successful. Results of this investigation test theoretical calculations, increase our understanding of higher lying electronic states of OH, and characterize the advantages and disadvantages of the new method.

BACKGROUND

ATMOSPHERIC STUDIES

The OH Meinel bands are a major component of infrared and near infrared light emitted by the earth's atmosphere between 75 and 105 km in the upper mesosphere, mesopause, and lower thermosphere at night.¹ OH emission occurs at slightly lower altitudes during the day.¹ The reaction of hydrogen atoms with ozone is the primary source of this emission; however, several alternative reactions have been hypothesized to explain the observed distribution of the emission over the various ground-state vibrational levels.² The emission is used to remotely measure the temperature of the mesosphere,³⁻⁶ infer concentration of other minor species,^{7,8} and monitor the propagation of gravity waves and other atmospheric phenomena through this region.⁹⁻¹² The rotational distribution, the absolute intensity, and the vibrational distribution all reveal information on the upper atmosphere.

LABORATORY AND THEORETICAL STUDIES

The vibrational band transition probabilities and the collisional energy transfer of the OH* in the ground electronic state are very important to the atmospheric modeling; however, disagreement in the values in the current literature makes conclusions drawn from these suspect. In this section, we will briefly summarize the available literature in both general areas.

Recently, two groups have published results on the dipole moment function in the ground state. These include a theoretical investigation by Warner et al.^{13,14} and an empirical parameterization using the available Meinel band intensity data of Turnbull and Lowe.¹⁵ The theoretical dipole moment function has been used to calculate tables of rotational-transition-specific lifetimes¹⁴ for many vibrational transitions in a manner similar to that initially presented in the classic work by Mies.¹⁶ For a complete discussion of the differences in the values, consult the recent manuscript by Turnbull and Lowe.¹⁵ In summary, the theoretical results and the results obtained from experiments disagree significantly in several of the transitions that are important in the upper atmosphere. The empirical dipole moment function is based on the best currently available spectroscopic data

on the relative magnitude of the vibrational band in the visible and the near infrared; however, experiments often disagree, and calibration over the entire wavelength region is difficult. The theoretical dipole moment function also relies on an experimental measurement¹⁷ of the dipole moment of $v = 0$ and shifts the results of the calculation slightly to make it agree.¹⁴ Which determination is the most accurate is still an open question, and further work in this area is needed.

The collisional energy transfer of OH* is as poorly understood as the transition probabilities, perhaps even more so. The experiments can be conveniently divided into those performed on high vibrational levels and those on low vibrational levels. Several groups (including our group) have measured the vibrational relaxation of the $v = 1$ and 2 levels of OH for a wide variety of collision partners.¹⁸⁻²⁵ The results are in relatively good agreement; where comparison is available, they vary by no more than a factor of two. For such diverse experiments this result is considered good agreement in the area of energy transfer. These lower vibrational levels are significantly easier to access than higher vibrational levels.

Chronologically the first experiments on OH vibrational dynamics were performed by Worley et al.²⁶ in 1972 and Streit and Johnson²⁷ in 1976 on high vibrational levels. They used the reaction of $H + O_3$ to generate the vibrationally excited OH. These pioneering experiments in the new field of vibrational energy transfer were subject to a fatal flaw. The inherent experimental difficulty was confirmed recently in two independent studies by Finlayson-Pitts et al.²⁸ and Greenblatt and Weisenfeld.²⁹ The complication is that the rate of the $H + O_3$ reaction, which produced OH in the $v = 9$ vibrational level, was slower than the rate of vibrational energy transfer that followed. Therefore, the simple kinetic analysis used in the previous studies was actually inapplicable. Because of this complication, the energy transfer measurements are probably in considerable error. A recent measurement²⁹ of the OH ($v = 9$) transfer rate by O_3 yields a value 20 times larger than that of the earlier studies. Eliminating the early data, we have few absolute measurements of the collisional removal rates. Finlayson-Pitts et al.²⁸ measured relative relaxation rates for $v = 9$ for the quenchers O_2 , CO_2 , and N_2 . The gap between the low v and high v has not been studied in detail. Absolute measurements are still needed for the high levels. The discharge flow methods used in Refs. 26 through 28 cannot unambiguously provide the needed state-to-state dynamic information.

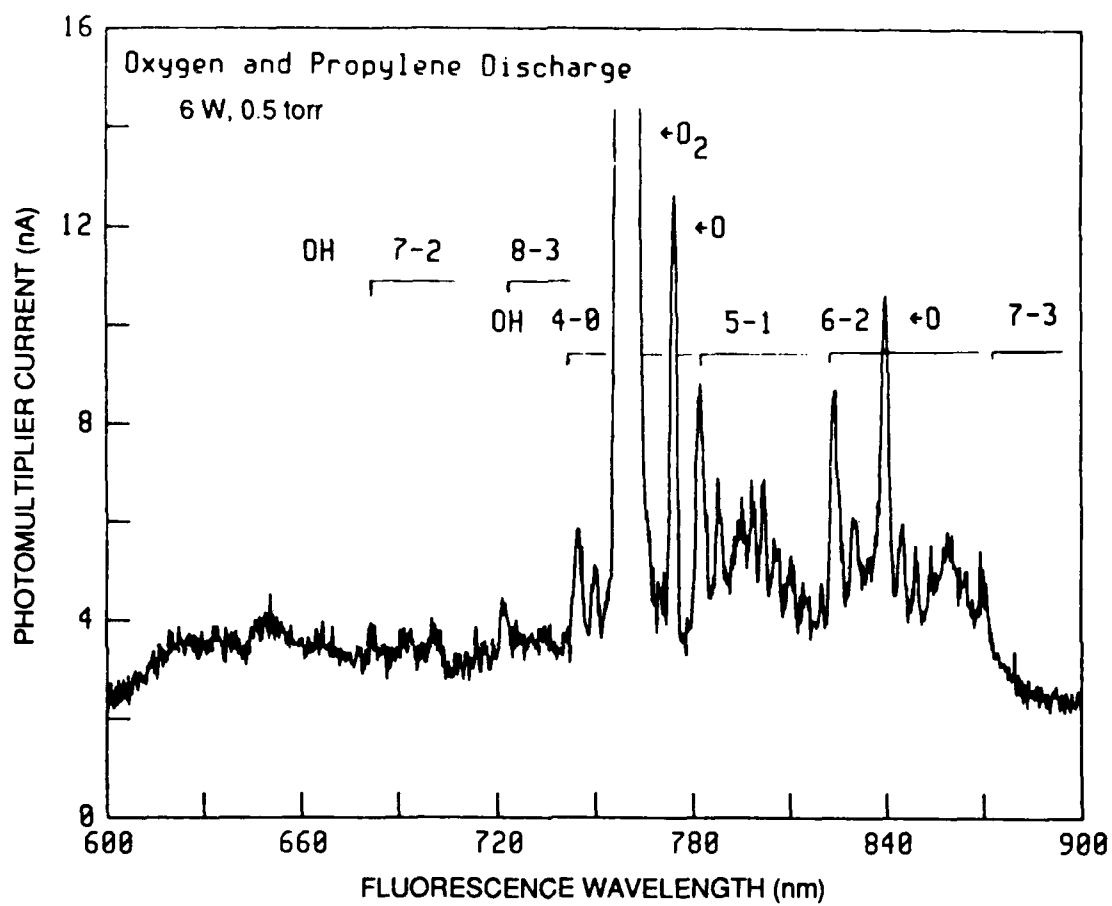
EXPERIMENTAL APPROACH

Our experimental approach can be conveniently subdivided into two sections. The first describes methods for producing the OH*, and the second describes the detection method itself. Both successful and unsuccessful attempts are outlined.

PRODUCTION OF OH*

OH in the upper atmosphere is in vibrational levels up to and including $v = 9$, which is over $25,000\text{ cm}^{-1}$ above the ground vibrational level. Clearly, thermal production of these levels is not feasible even in the high temperature environment of flames.³⁰ For accessing levels up to $v = 9$, reaction methods appear the most promising. The same reaction, hydrogen atoms plus ozone, that generates OH* in the earth's atmosphere can be used in the laboratory to generate OH in vibrational levels up to $v = 9$. Another complex reaction method involving oxygen atoms plus propylene (C_3H_6) also produces OH* up to $v = 10$, mostly likely through the fundamental reaction step, $\text{O} + \text{HCO}$.³¹ The latter method was attempted initially because we had a stainless steel flow cell whose geometry and construction materials were not conducive to use with ozone.

Oxygen atoms were generated by a microwave discharge through an O_2 and helium mixture or pure O_2 . Downstream from the discharge in the flow cell we added propylene. Using this method, we observed Meinel band emission from OH* between about 600 and 900 nm. Figure 1 is the chemiluminescence downstream of a 0.5-Torr pure O_2 discharge at 6 W input power with a trace of added C_3H_6 . The emission was collected by a two-lens optical system, dispersed by a 0.3-m monochromator, and detected by a cooled red-sensitive photomultiplier tube (RCA 31034). The output of the photomultiplier was measured with a logarithmic picoammeter and recorded in a computer. The computer also scanned the monochromator. Features in the spectrum can be attributed to $\text{OH}(X^2\Pi_i)$ vibrational levels up to $v = 8$, with the strongest being assigned to $v' = 5$ and 6. In addition to the OH Meinel band features, a high intensity O_2 band was observed along with two O atom lines (labeled in Figure 1). We maximized the emission from the (6,2) vibrational band by adjusting the relative flows of the gases, total pressure, and distance to the propylene injector. Figure 1 shows the data under conditions close to optimum.



RA-3772-7

Figure 1. Chemiluminescence downstream of an oxygen discharge with added propylene. Most features are due to OH* emission. Signals are also observed from electronically excited oxygen atoms and molecules.

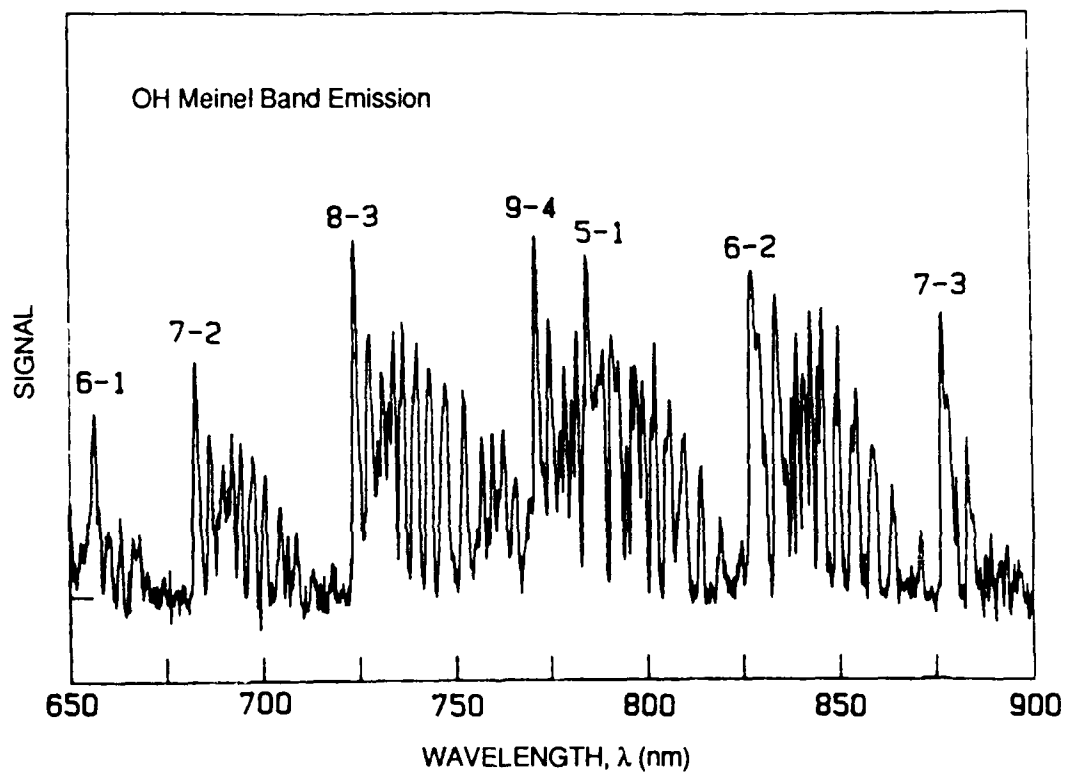
Butylenes gave signals comparable to those for propylene, while ethylene gave significantly less vibrationally excited OH signals.

After assembly and construction of a suitable flow cell, we used the reaction of $\text{H} + \text{O}_3$ to generate high concentrations of OH^* . The H atoms were generated by passing He or Ar with a small seeding of H_2 through a microwave discharge delivering about 30 W. A small flow of ozone in He or Ar was injected just above the observation region. Under all conditions helium and argon carrier gas was in excess. The ozone was generated before the experiments with a commercial ozonizer and stored on silica gel at 195 K. Again the production of OH^* was maximized by observing Meinel band emission in the visible spectrum by using a red-sensitive photomultiplier tube. A sample spectrum of the emission dispersed by a monochromator is shown in Figure 2. We observed strong signals from ground-state vibrational levels ranging from $v = 5$ to 9.

As can be seen from a comparison of the signal-to-noise ratio on the spectra in Figures 1 and 2, more OH^* is generated by the $\text{H} + \text{O}_3$ reaction. We estimate almost a factor of 100 difference. Such comparisons depend on many different parameters, for example differences in the flow cell and flow conditions; therefore, a detailed comparison was not made. We believe the $\text{H} + \text{O}_3$ reaction generates significantly more OH, and it was the only source for which we observed LIF signals.

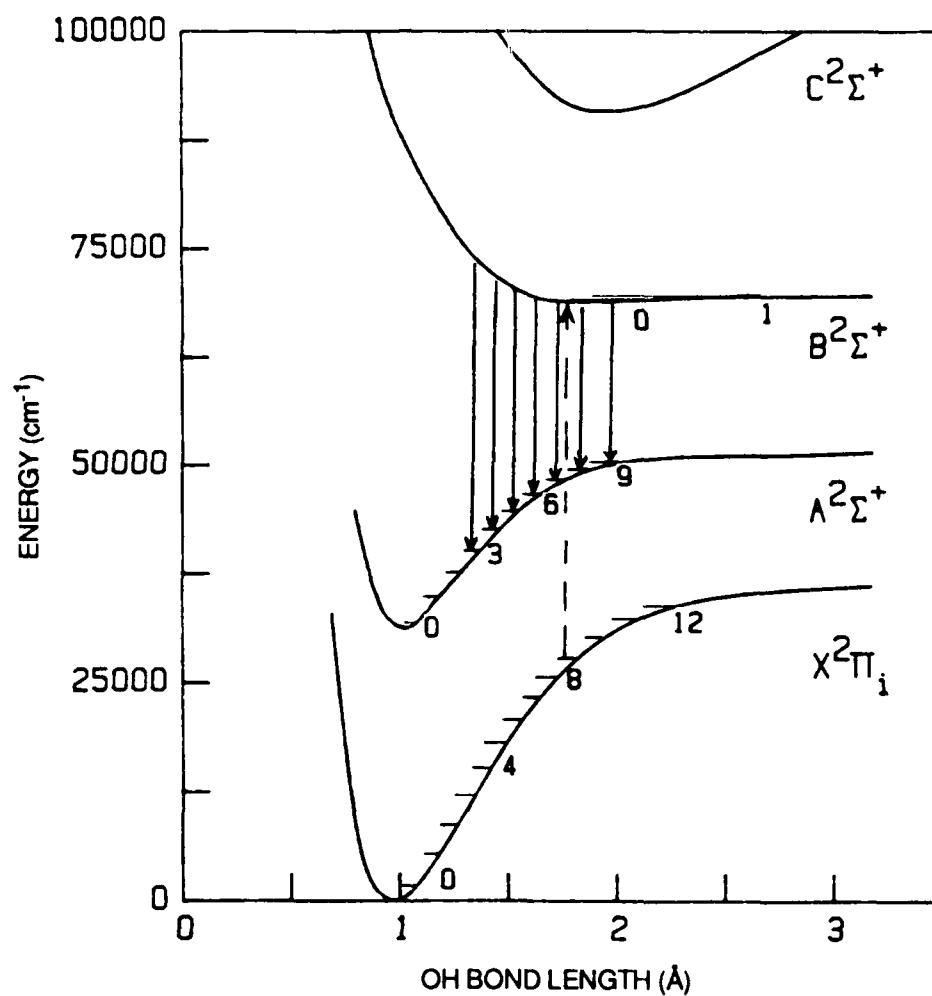
DETECTION OF OH^*

High-lying vibrational levels in the ground state of OH can be detected by means of the $\text{B}^2\Sigma^+ - \text{X}^2\Pi_i$ electronic transition. A recent theoretical calculation by Langhoff et al.³² indicates this excitation is feasible with new laser technology. Figure 3 shows the potential energy curves for the $\text{X}^2\Pi_i$, $\text{A}^2\Sigma^+$, $\text{B}^2\Sigma^+$, and $\text{C}^2\Sigma^+$ electronic states of OH. The curves, constructed from the data in Ref. 32, show that the equilibrium bond lengths for the lowest lying vibrational states of the X and A states are very different from those for the B and C states. Interestingly, the B state has a very shallow potential well containing only two vibrational levels. Because of the Franck-Condon principle, the only strong transitions to the B state are from high-lying vibrational levels of the ground state and the A state. The B-A transition has been observed in discharges in H_2O ;³³⁻³⁵ however, until this investigation, the B-X transition had not been seen. In Figure 3, the dashed line shows the excitation by means of the B-X (0,8) vibrational band, and the solid lines show that the $\text{B } v' = 0$ state will fluoresce to several levels in the A state at longer wavelengths. This situation is ideal for LIF detection; a weak transition is excited with a powerful laser, and a strong fluorescence transition in a very different wavelength region is monitored.



RA-3772-8

Figure 2. OH^* Chemiluminescence from the reaction of $\text{H} + \text{O}_3$ in a discharge flow cell. Each vibrational band is labeled near the corresponding R head feature.



RA-3772-9

Figure 3. OH potential energy curves for the four lowest doublet states. The dashed line shows excitation via the $B^2\Sigma^+ - X^2\Pi_i$ (0,8) band near 226 nm, while the solid lines illustrate the strong fluorescence to the A state.

Problems with scattered light or a need to look near the excitation laser wavelength are minimized.

Appendix A is a preprint of a manuscript describing the experimental procedure for B-X LIF detection is described in detail. The experimental approach is only outlined briefly here. Light between 210 and 230 nm from a frequency-doubled excimer-pumped dye laser was used to excite the OH molecules from the ground electronic state to the B state. A β -barium borate doubling crystal was used to frequency-double the light, generating about 1 mJ. We separated the doubled light from the fundamental with a Pellin-Broca prism and directed the beam through the flow cell with dichroic mirrors. The cell was designed so we could observe the fluorescence from two sides. On one side we used a two-lens system and imaged the fluorescence onto a slit of a 0.3-m monochromator, and on the other we used a lens and several colored glass and interference filters to select a region of the visible spectrum. When the monochromator was scanned, the second side could be used to monitor the total signal and thereby to account for drifts in the laser power, laser wavelength, and OH production source. Figure 1 of Appendix A shows an excitation spectrum taken by scanning the laser from 224.8 to 225.8 nm of the previously unobserved (0,8) vibrational band of the B-X system. The B-A fluorescence near 500 nm in the (0,7) band was monitored. The signal was very large and yielded a good signal-to-noise ratio. We were able to excite (0,8), (1,8), and (0,9) vibrational bands in the B-X electronic system. We attempted to look for the OH (0,10) band, but no signals were observed. Other vibrational bands could be excited, but because they would not provide any new spectroscopic information so they were not investigated in this study. The positions for all the rotational lines could be calculated from the available spectroscopic constants.³³⁻³⁶ No new spectroscopic information on line position and constants was obtained from the data.

The experiments described above were successful because a significant amount of OH* was produced in the reaction of H + O₃ and the laser pulse energy was about 1 mJ near 225 nm with a 100-Hz repetition rate. Earlier in the project, we unsuccessfully attempted to detect the OH* with a laser that had a factor of 10 less power and a repetition rate 10 times slower. This attempt was made using the much less efficient O + C₃H₈ source. During these experiments we could not see B-X LIF signal. At the same time and with the same source, we attempted an alternative method of detection of OH*. Briefly, we tried to excite the OH $v = 9$ molecules to the $v = 13$ level by using an infrared photon. According to theoretical calculations,¹⁴ this transition is very strong and could be saturated with the available pulsed Raman-shifted output of a Nd-YAG pumped dye laser. The

infrared method would rely on efficient transfer of vibrational to electronic energy, from $v = 13$ to the $A^2\Sigma^+$ electronic state ($v = 13$ lies slightly higher in energy than $v = 0$ of the A state). All the vibrational levels directly populated by the reaction $H + O_3$ do not have enough energy to reach the A electronic state. We expected little background light near the A-X band of OH. If ultraviolet fluorescence was observed, we would obtain both population information on $v = 9$ and total relaxation information on $v = 13$. Unfortunately, the vibrational levels above $v = 10$ have never been observed spectroscopically and the energy transfer process, though judged feasible from basic principles and our knowledge of A state collisional quenching, is heretofore uncharacterized. Experimental values for the spectroscopic constants of $v = 9$ and estimates of the values for $v = 13$ were used to predict the absolute wavelength position and rotational structure of the band.

Before these experiments, we had hoped the OH production source would be relatively "dark" in the region of the A-X electronic transition in OH. However, after examination of the discharge that gave significant Meinel band emission, we observed a large amount of light corresponding to A-X OH emission. Preliminary results of analysis of its strength relative to that of the Meinel emission indicate that this A-X emission was due to the energy pooling collision of two vibrationally excited OH molecules. The A-X emission increased more than linearly with the Meinel band emission intensity. This result *limited our detection sensitivity and increased the noise*. Both with this production source and the $H + O_3$ reaction, the A-X emission is strong when the OH* emission is strong.

Briefly, the Raman-shifted output of the dye laser, with about 0.5 to 2.0 mJ per pulse, was used to excite the OH*. While scanning the wavelength between about 1.35 and 1.45 μm , we observed no enhancement in the A-X signal after the laser pulse. We examined different discharge conditions, added efficient collision partners for vibrational energy transfer, and scanned over a wide wavelength region, but we observed no signal. With a more intense source of OH* like $H + O_3$ these experiments might work, but they were never attempted. This method might provide a useful method of looking at the dynamics of higher levels, but with the development of the B-X method, it is less important.

RESULTS

Spectroscopic information must be extracted before B-X LIF is used as a quantitative diagnostic of high vibrational levels. We obtained values for the relative vibrational band transition strengths in the B-A and B-X transitions, the fluorescence lifetimes of the B state, and the behavior of the B state during collisions. These measurements also provide a stringent test of theoretical calculations on the OH radical.

RELATIVE VIBRATIONAL BAND TRANSITION PROBABILITIES

The vibrational band transition probability measurements are described in detail in Appendix A and only will be briefly described here. In the experiment, we dispersed the fluorescence and measured the relative intensity of the vibrational bands of the B-A electronic transition for the two bound vibrational levels of the B state. Figure 2 of Appendix A shows the fluorescence spectra from both $v = 0$ and 1 corrected for the monochromator response. The fraction of the total fluorescence from a given vibrational level in the B state into each vibrational level of the A state is presented in Table 1 of Appendix A. A direct comparison to a theoretical calculation of Langhoff et al.³² is also presented in that table. The theoretical and experimental results are in good agreement. Most of the band strengths agree within 10%, which is less than the experimental error and much less than the combined precision of such an experiment and the expected uncertainty in the calculation. Our measurements are also in reasonable agreement with previous experimental studies of the strong bands from B $v' = 0$ found in Refs. 33 and 35.

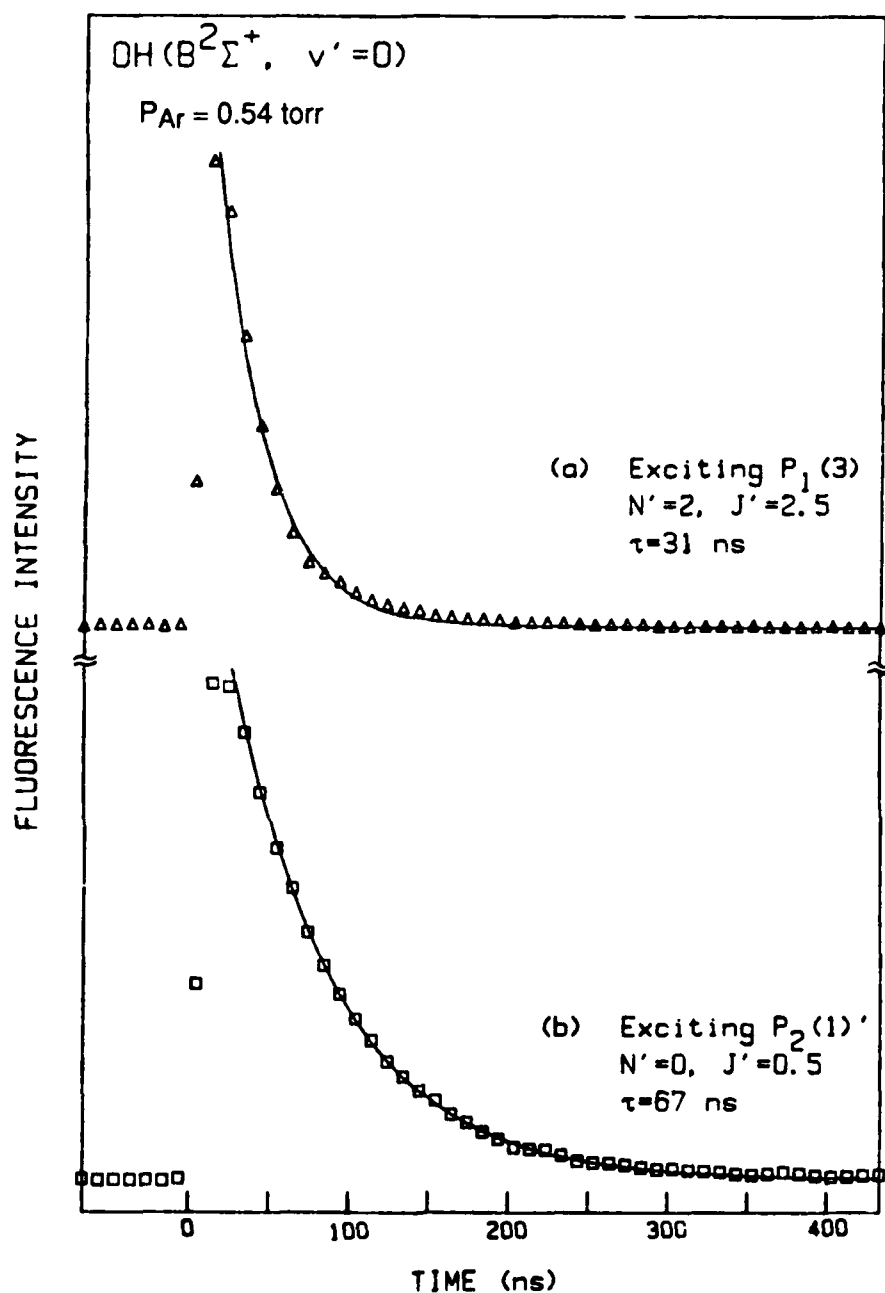
We also observed fluorescence from the B-X (0,9) and (0,10) vibrational bands. Figure 3 of Appendix A shows a fluorescence spectrum in the region of the B-X (0,10) and B-A (0,3) bands obtained by exciting the B-X (0,8) band. From these data, we can extract the first experimental information on the relative strengths of the B-A and B-X transitions. The result is a ratio, $I[\text{B-A (0,3)}]/I[\text{B-X (0,10)}] = 1.6 \pm 0.5$. The B-X transition is much weaker than the B-A transition, as evidenced by the comparable intensities of the (0,10) band of the B-X transition, which is one of the stronger bands in this transition and the very weak (0,3) band of B-A (see Figure 3 and Table 1 of Appendix A). The total emission transition probability into all vibrational levels is computed³² to be about a factor of 17 higher for B-A than for B-X, but in the latter system the transitions are

spread over a larger number of bands, so a strong B-X band is about a hundredfold weaker than a strong B-A band. The above ratio can be compared to the theoretical result of 0.5. The theoretical results for this ratio differ from the experimental values by more than the error bars. This large difference may be due to the difficulty of calculating a realistic empirical potential for high vibrational levels ($v \geq 10$) of OH, $X^2\Pi_i$ (see Figure 1 in Ref. 32) and the proximity of the electronic transition moment of B-X to its zero crossing in this region. Calculations of these weak transitions are difficult and involve the relative magnitude of two different electronic transition moments.

FLUORESCENCE LIFETIMES OF B STATE

The fluorescence lifetime of the B state has been the subject of disagreement in the literature. The only experimental measurement by Bergeman et al.³⁵ extracted values of 2000 ± 700 ns for $v' = 0$ and 3000 ± 1000 ns for $v' = 1$. Theoretical calculations³² that agree well for the relative vibrational band transition probabilities of the B-A transition produce values of 300 ± 70 ns for $v' = 0$ and 510 ± 100 ns for $v' = 1$. The values disagree by more than a factor of 5. The experimental study of Bergeman et al.³⁵ used an electron beam through water vapor to generate electronically excited OH and was not a direct measurement. With our technique of laser excitation, we can record the time evolution after excitation of a single vibrational and rotational level of the B state as a function of pressure and thereby extract the fluorescence lifetimes in a straightforward manner.

To obtain accurate fluorescence lifetimes, we monitored fluorescence from an entire vibrational band of the B-A electronic transition by using a filtered phototube. For $v' = 0$ we monitored the (0,7) band, and for $v' = 1$ we selected the (1,9) band. The amplified output of the photomultiplier was captured by a transient digitizer to record the time evolution of the laser-induced fluorescence from the B state. Figure 4 shows two typical signals. The boxes and triangles are the experimental data points taken every 10 ns, and the solid line is the best fit single exponential to the time decay from 90% to 10% of the peak value. The fluorescence decays seem adequately represented by a single exponential even though (as will be shown) below the data are actually composed of several exponentials of similar magnitude. Both traces were obtained under identical discharge conditions that excited either the $P_1(3)$ transition (upper trace) or the $P_2(1')$ transition (lower trace) of the B-X (0,8) band. The fluorescence from both states decays rapidly, with the $J' = 2.5$, $N' = 2$ state fluorescence (upper trace) decaying about twice as fast as that from the $J' = 0.5$, $N' = 0$ state (lower trace).



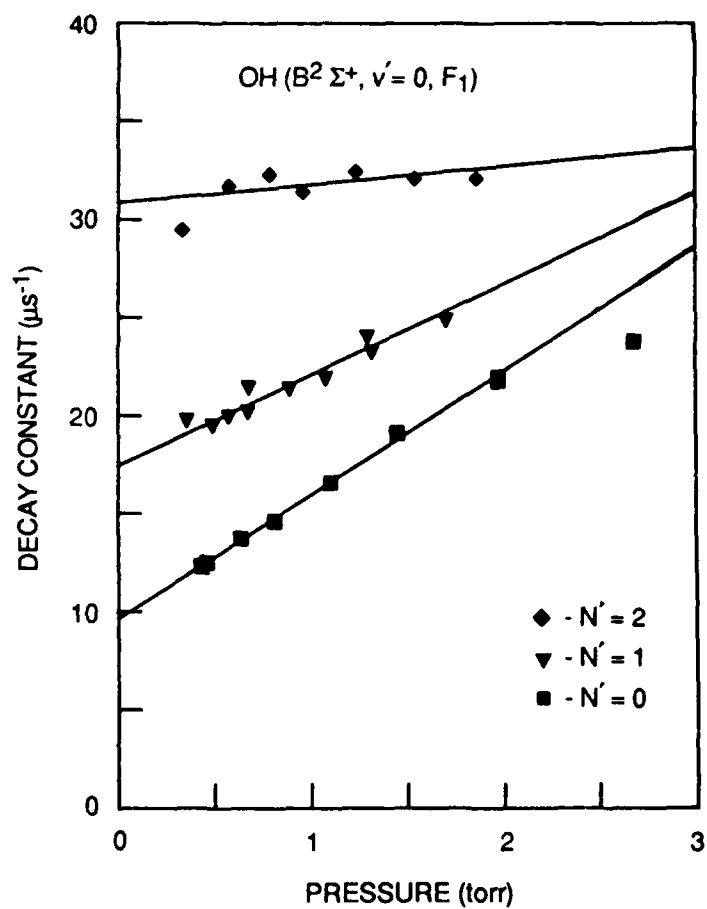
RA-3772-10

Figure 4. Time evolution of the B-X LIF signal after excitation of two different rotational levels in $\text{OH} (\text{B}^2\Sigma^+, v' = 0)$. The boxes and triangles are the experimental data, and the solid line is the best fit single exponential between 90% and 10% of the peak value.

Before further discussion of the pressure dependence of the temporal evolution of the LIF signals, a brief discussion of the fine structure of the B state is needed to understand the experiments and results. The B state has no orbital angular momentum but does have an unpaired electron that gives it a spin of $1/2$. Therefore, all rotational levels with the rotational quantum number N greater than zero are doubled by the two possible orientations of the spin with respect to the rotational angular momentum. These are labeled the F_1 and F_2 components and are very close in energy. In the A state, the F_2 component is at slightly lower energy for a given N . The sign of the spin-rotation coefficient in the B state is as yet undetermined, so the relative position of the two states is unknown. Often these two levels can have different fluorescence lifetimes as a result of coupling with a predissociating state, as is described below. Depending on the P, Q, or R branch excited, either a mixture of both F_1 and F_2 levels or pure F_1 and F_2 levels are populated. The fraction of either the F_1 or F_2 level excited for a rotational transition can be calculated from the spectroscopic constants³⁶ if the laser power is not high enough to saturate the transition.

Several control experiments had to be performed before we could study the pressure dependence of the LIF. Initially, we had to determine if the residual gases and species from the production of the OH^* had any effect on the time-dependent signals. A series of experiments was conducted in which the partial pressure of H_2 in the cell was varied by more than an order of magnitude (from about 10 to 200 mTorr) to determine its effect on the measured time decay. Over the range of H_2 partial pressures investigated, the decay constant increased by only 10%. We always operate at a H_2 partial pressure less than 25 mTorr which makes a negligible contribution to the lifetime. A similar series of experiments was performed to determine the effect of the O_3 partial pressure. In this set of experiments, the total pressure of the cell was maintained at ~ 500 mTorr by adjusting the flow of buffer gas through the discharge. This adjustment was required because the O_3 was added to the cell in a flow of the same buffer gas. In these experiments, the Ar/O_3 flow was varied by more than an order of magnitude, and there was a 10% increase in the range of values we obtained for the decay constant. These experiments show that the minor components of the total gas mixture do not contribute to the time dependence at the level of the uncertainty of the measurements.

Figure 5 summarizes the pressure dependence of the fluorescence decay constants for F_1 levels with $N' = 0, 1$, and 2 with helium as the collider. From the intercept to a first approximation, we can obtain the fluorescence lifetime, and from the slope, we obtain collisional energy transfer information. As can be seen in Figure 5, both the slopes and the



RA-3772-3

Figure 5. Plot of the decay constant for LIF after excitation of different rotational levels in OH($B^2 \Sigma^+$, $v' = 0$, F_1) versus the helium pressure.

intercepts of the lines are different depending on the excited rotational level. The different values for the intercept of the different rotational levels indicate a previously unobserved predissociation of this state. The preliminary fluorescence lifetimes (i.e., the inverse of the intercept) are given in Table 1. We will discuss the accuracy of this measurement below. The uncertainties given in Table 1 are two standard deviations from the unweighted fit of the decay constants by the method of linear least squares.

Because of overlaps in the excitation spectrum in the B-X(0,8) band, we could not excite only the F₂ component of the low rotational levels in $v = 0$. We could only populate these levels by using transitions that also excite the F₁ component. Exciting these overlapping transitions clearly showed that the F₂ component for the same N is much longer lived than the corresponding F₁ component. Extraction of the fluorescence lifetime for the F₂ component from an overlapped excitation feature requires a more complicated analysis. For this analysis, we have applied two methods, a complete kinetic simulation, as described below, and a simple subtraction method outlined here. From the spectroscopic constants for the transition in question, we can calculate the relative amounts of the F₁ and F₂ components we excite in the overlapped feature. For example, for the overlapping Q₁(1) and QP₂₁ transitions, we excite 55% F₁ and 45% F₂ of the same N' in the excited state. We also know the time dependence of the F₁ component from direct excitation. We take the initial amplitude at the time of the laser pulse and subtract the relative amplitude of the F₁ contribution with its corresponding single exponential decay from the total signal. We fit the remaining amplitude from 90% to 10% of the peak as described above and attribute that to the F₂ component. The decay constant is then plotted as a function of collider pressure exactly as before, with the intercept giving information on the fluorescence lifetime. This approach gives the values for the F₂ component given in Table 1. Several approximations go into this extraction; we have attempted to determine these approximations by using a kinetic model, described below.

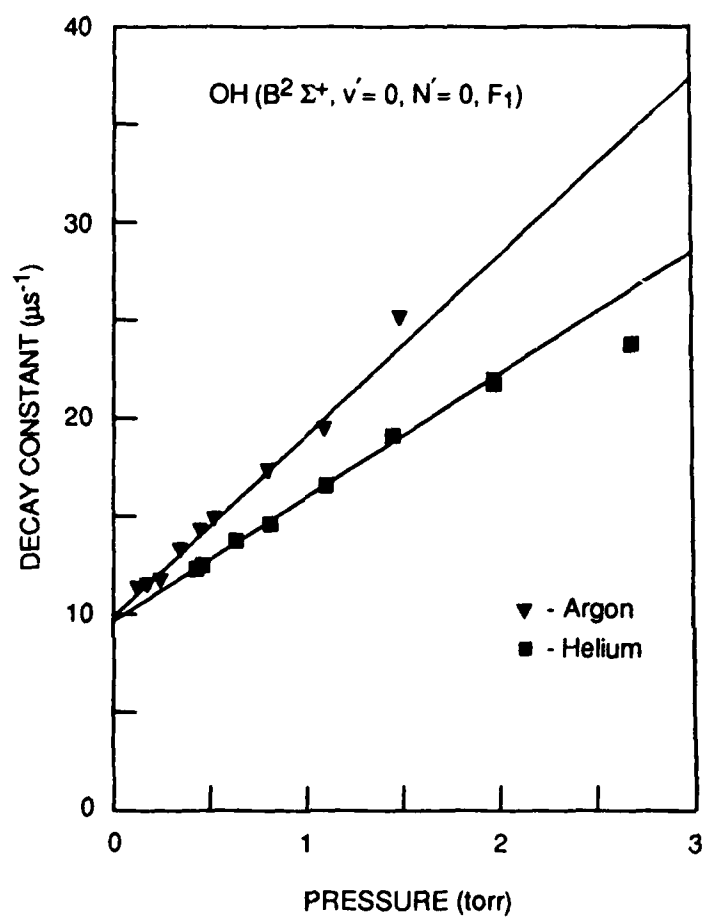
We examined the $v' = 0$ level by using both helium and argon as the primary buffer gas. In all cases, we obtained measurements that agree within the respective errors. Figure 6 shows the data after excitation of $J' = 0.5$, $N' = 0$ for both Ar and He collider. The lines have different slopes, which indicate different rate constants for the collisional processes but very similar intercepts. These results show directly that Ar is more efficient than He in rotational energy transfer (RET) in the B state of OH. Figure 1 of Appendix B shows the data after excitation of $v' = 0$ and $v' = 1$ with the same rotational quantum number. The slopes are similar but the intercepts are different, with the $v' = 0$ level being longer lived than the $v' = 1$ vibrational level. In $v' = 1$, $N' = 2$ we could excite only F₁ and F₂ levels;

Table 1. Fluorescence lifetimes of OH($B^2\Sigma^+$) extracted from the intercept of plots of fluorescence decay constant versus pressure.^a

	$v' = 0$		$v' = 1$	
	F_1	F_2^b	F_1	F_2^b
$N = 0$	102 ± 7	---	71 ± 5	
$N = 1$	60 ± 3	108 ± 24	37 ± 1	110 ± 25
$N = 2$	27 ± 2	67 ± 9	15 ± 1	32 ± 2

^aUnits of nanoseconds. Errors are the statistical two standard deviations of the best linear fit to decay constant data.

^b F_2 values are obtained from simultaneous excitation of F_1 and F_2 components.



RA-3772-4A

Figure 6. Plot of the decay constant versus rare gas pressure.
The $v' = 0$, $N' = 0$, F_1 level in the $B^2 \Sigma^+$ state was excited.

we observed that the F_2 levels for a given N are significantly longer lived than the corresponding F_1 levels (Figure 7).

The accuracy of the fluorescence lifetimes is difficult to assess without some knowledge of the collisional energy transfer processes that are occurring. We must examine the pressure dependence and see what is responsible for the very different slopes of the lines for different rotational levels in Figure 5. In the $v' = 0$ level of the B state, two basic energy transfer processes can occur in collisions of the excited OH with He: The OH molecules could be removed from the excited electronic state either to a lower lying state of OH or through direct collision-induced dissociation. In direct collision-induced dissociation, the B-state OH collides with the He and exits via a repulsive surface. The OH molecules could also undergo rotational energy transfer (RET) within the $v' = 0$ level of the B state. Under most circumstances, such RET collisions do not result in an increase in the decay constant (the time dependence) of the LIF signal. However, if that state predissociates more rapidly than the initial state, the time dependence of the fluorescence is shortened. Also, if the level is shorter lived than the surrounding rotational levels, then increasing the pressure of the collider gas will have little effect on the time decay and may in some cases make the fluorescence longer lived (see $N' = 2$ in Figure 5). Which process is occurring in the B state of OH? Clearly, from Figure 5, the slopes of the lines change markedly with N' . The slope of the line that can be described as a phenomenological rate constant decreases with increasing N' . Values of the slopes of the lines are presented in Table 2. In the A state of OH, where no predissociation occurs in $v = 0$ there is evidence for a decrease in the removal with increasing rotational level for molecular colliders.³⁷ However, the effects were not as dramatic as observed here. Also for the A state of OH, both He and Ar were very poor quenchers of OH. Therefore, we believe He will also be inefficient at quenching the B state. The explanation lies in RET coupled with predissociation of the levels, as described above. Resolved fluorescence scans indicate that some RET has occurred, and the magnitude of the rate constants is typical of RET. Therefore, analysis of the slopes is not straightforward and requires a kinetic model to evaluate its accuracy.

A model of this fluorescence must include radiation, quenching, predissociation, and rotational energy transfer. The most difficult component to implement is RET. The number of rotational-level-specific rate constants between individual levels becomes unmanageable quickly. To model the system, we choose to apply the infinite order sudden scaling relationship derived by Alexander³⁸ for collisions of a $^2\Sigma$ molecule with a structureless atom. With these scaling relationships, all RET rate constants can be

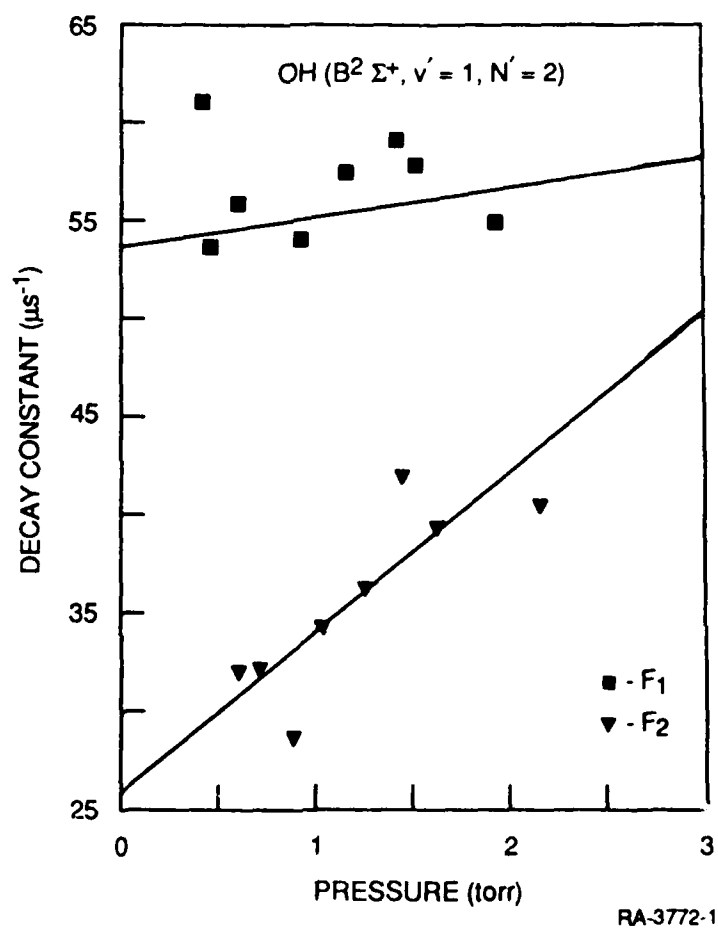


Figure 7. Plot of the decay constant versus helium pressure after excitation of different fine-structured levels in OH ($B^2 \Sigma^+, v' = 1, N' = 2$).

Table 2. Slopes of the plots of fluorescence decay constants versus pressure for excitation of several vibrational and rotational levels in the $B^2\Sigma^+$ state of OH.^a

	$v' = 0$		$v' = 1$	
	F_1	F_2^b	F_1	F_2^b
$N = 0$	5.9 ± 0.4 [8.9 ± 0.5]		6.6 ± 0.4	
$N = 1$	6.0 ± 0.6 [5.0 ± 0.3]	6.9 ± 0.3 [8 ± 2]	9 ± 1	10 ± 2
$N = 2$	2 ± 1 [-1 ± 1]	4 ± 1 [5.5 ± 0.7]	-1 ± 2	6 ± 2

^aUnits of $\mu\text{s}^{-1} \text{Torr}^{-1}$. Errors are the statistical two standard deviations of the best linear fit to decay constant data.

^b F_2 values are obtained from simultaneous excitation of F_1 and F_2 components.

calculated from a limited number of base rates. In this way the number of independent variables can be reduced. The following equation is used to calculate the state-to-state RET rate constants:

$$k_{J,\epsilon \rightarrow J',\epsilon'} = \exp[-\Delta/kT](2J' + 1) \sum_{\ell} (2\ell + 1) \frac{1}{2} [1 - \epsilon\epsilon'(-1)^{J+J'+\ell}] \begin{pmatrix} J' & \ell & J \\ \frac{1}{2} & 0 & \frac{1}{2} \end{pmatrix}^2 k_{\ell+\frac{1}{2}\epsilon \rightarrow \frac{1}{2}\epsilon'}$$

where the primes indicate final states and the unprimed values the initial state, the variable Δ is equal to zero if the initial state is higher in energy than the initial rotational state (this factor is used to make the rates obey detailed balance), J is the total angular momentum, $\epsilon = +1$ for F_2 levels, and $\epsilon = -1$ for F_1 levels and ℓ is the summation index for the base rates. The variable ℓ can take integer values. The numbers in the large parentheses are a conventional 3-j symbol.³⁸ With this expression, all rate constants can be estimated from a set of base rates $[\sum_{\ell} k_{\ell+\frac{1}{2}\epsilon \rightarrow \frac{1}{2}\epsilon'}]$.

This model is used to access the accuracy of the preceding analysis. Initially, we use the radiative lifetime derived from theory³² and the fluorescence lifetime obtained from the intercepts to obtain the predissociation rate; we assume no electronic quenching. Using a gradient search nonlinear least squares fitting routine, we obtain the best fit value of the single quantum base rate, $k_{\frac{3}{2}\epsilon \rightarrow \frac{1}{2}\epsilon}$, setting all other base rates to zero and fixing all the predissociation rates to the values extracted from the intercepts. From this fit we obtain a reasonable representation of the RET. The program also calculates synthesized time dependences for comparison with the experimental values. We then fit these synthesized data in the same manner described above to see if we can extract the input fluorescence lifetimes. In most cases the values agree to within 20%. We believe the best values for the radiative lifetimes would have to be corrected for these systematic differences. Such corrections are currently under way for $v' = 0$. A similar analysis will be performed on the data for $v' = 1$. The values in Table 1 should be considered preliminary numbers.

Values for the base rates within the infinite-order sudden framework will also be extracted from the time dependence of the signals. These values will facilitate comparison of the RETs in He and Ar and in $v' = 0$ and $v' = 1$. A preliminary number for the base rate $k_{\frac{3}{2}\epsilon \rightarrow \frac{1}{2}\epsilon}$ for $v' = 0$ in He is $\sim 3 \times 10^{-10} \text{ cm}^3 \text{ s}^{-1}$. Because of the coupling of the predissociation with the rotational energy transfer, the analysis is complex and assigning an uncertainty to these measurements is therefore difficult. The results of this fitting will be described in detail in an upcoming publication.

ADVANTAGES AND DISADVANTAGES OF B-X LIF

With the information gleaned from the above results, we can assess the usefulness of the B-X LIF method for the detection of vibrationally excited OH. Several advantages and disadvantages became apparent in this study. The most important conclusion is that the signals are large and the emission characteristics of the OH are adequately described by theoretical calculations.³² With the wavelength dependence of the fluorescence obtained by this method, we can select the best detection method for future experiments. From the values for the B-X vibrational band transition probabilities given in Ref. 32, we estimate it should be feasible to probe vibrational levels in the ground state from about $v' = 6$ to the highest bound vibrational levels. Interestingly, some of these levels have never been observed for OH. The time resolution of this probe is also a distinct advantage. It can take a 10-ns picture of the concentration of OH in a specific vibrational and rotational level. This property is extremely important in designing new experiments to measure the vibrational and rotational energy transfer in the ground state.

However, the technique also has at least one important disadvantage, the predissociation of the B state. This rotational and fine-structure dependent effect makes measuring rotational distributions difficult and may limit the range of rotational levels that can be investigated. It also reduces the number of fluorescent photons, but in most cases the signal levels would be sufficient. This is not an insurmountable problem. A careful study at low pressure on a rotationally equilibrated sample would help clarify the dependence of the predissociation on the OH.

Overall, we feel this method will be extremely useful in the study of vibrational transfer in the ground state.

CONCLUSIONS

From the above data, we can state with confidence that the $B^2\Sigma^+-X^2\Pi_i$ LIF method will be a useful diagnostic tool for investigating the high vibrational levels ($6 \leq v \leq 15$) in ground-state OH. In addition, this study has been a rigorous test of OH theoretical calculations³² by our examination of the relative transition probabilities of the B-A and B-X bands. We were extremely encouraged by the good agreement between the experimental results and theoretical calculations on this system. We have also shown that the fluorescence lifetimes of the B state of OH are indeed shorter than previously measured experimentally. This result clears up a troublesome disagreement between experimental³⁵ and theoretical³² measurements on this quantity. With this sensitive and state-selective technique, a detailed study of the collision dynamics of high vibrational levels important in the upper atmosphere can be undertaken.

MANUSCRIPTS, PRESENTATIONS, AND PERSONNEL

MANUSCRIPTS

The following manuscripts have been or will be completed under this contract:

1. A. D. Sappey, D. R. Crosley, and R. A. Copeland, "Laser-Induced Fluorescence of the $B^2\Sigma^+-X^2\Pi_i$ System of OH: Detection of $v'' = 8$ and 9 ," *J. Chem. Phys.*, in press.
2. A. D. Sappey, D. R. Crosley, and R. A. Copeland, "Laser-Induced Fluorescence in the $B^2\Sigma^+-X^2\Pi_i$ System of OH," in *Advances in Laser Science-IV*, W. C. Stwalley and M. Lapp, editors, AIP Conference Proceedings xxx, xxx (American Institute of Physics, New York, 1989).
3. A. D. Sappey and R. A. Copeland, "Laser-Induced Fluorescence in the $B^2\Sigma^+-X^2\Pi_i$ System of OH: Fluorescence Lifetimes and Collision Dynamics of the B State," *J. Chem. Phys.*, in preparation.

The first two of these papers are included here as Appendix A and B.

PRESENTATIONS

The following presentations have been made on this contract:

1. A. D. Sappey, D. R. Crosley, and R. A. Copeland, "Laser-Induced Fluorescence in the $B^2\Sigma^+-X^2\Pi_i$ System of OH," Fourth International Laser Science Conference, Atlanta, Georgia, October, 1988. [*Bull. Amer. Phys. Soc.* 33, 1640 (1988).]
2. A. D. Sappey, D. R. Crosley, and R. A. Copeland, "Laser-Induced Fluorescence of the $B^2\Sigma^+-X^2\Pi_i$ System of OH: Detection of $v'' = 8$ and 9 ," Thirty-Sixth Annual Conference on Modern Spectroscopy, Asilomar, California, January, 1989.

PERSONNEL

The work on this contract has been performed by Andrew Sappey, David Crosley, and Richard Copeland, all of whom are members of the Molecular Physics Laboratory of SRI International.

REFERENCES

1. E. J. Llewellyn, B. H. Long, and B. H. Solheim, "The Quenching of OH* in the Atmosphere," *Planet. Space Sci.* **26**, 525 (1978).
2. J. A. Kaye, "On the Possible Role of the Reaction $O + HO_2 \rightarrow OH + O_2$ in OH Airglow," *J. Geophys. Res.* **93**, 285 (1988).
3. V. I. Krassovsky and N. N. Shefov, "The Intensities, Doppler and Rotational Temperatures of the Upper Atmospheric Emissions and Internal Gravity Waves," *Ann. Geophys.* **32**, 43 (1976).
4. J. F. Noxon, "Effect of Internal Gravity Waves Upon Night Airglow Temperatures," *Geophys. Res. Lett.* **5**, 25 (1978).
5. G. G. Sivjee and R. M. Hamwey, "Temperature and Chemistry of the Polar Mesopause OH," *J. Geophys. Res.* **92**, 4663 (1987).
6. W. Pendleton, Jr., P. Espy, D. Baker, A. Steed, M. Fetrow, and K. Henriksen, "Observation of OH Meinel (7,4) P(N" = 13) Transitions in the Night Airglow," *J. Geophys. Res.*, in press.
7. W. F. J. Evans and E. J. Llewellyn, "Atomic Hydrogen Concentrations in the Mesosphere and the Hydroxyl Emissions," *J. Geophys. Res.* **78**, 323 (1973).
8. I. C. McDade and E. J. Llewellyn, "Mesospheric Oxygen Atom Densities Inferred from Night-Time OH Meinel Band Emission Rates," *Planet. Space Sci.* **36**, 897 (1988).
9. V. I. Krassovsky, B. P. Potapov, A. I. Semenov, M. V. Shagaev, N. N. Shefov, V. G. Sobolev, and T. I. Toroshelidze, "Internal Gravity Waves Near the Mesopause and the Hydroxyl Emission," *Ann. Geophys.* **33**, 347 (1977).
10. R. L. Walterscheid, G. G. Sivjee, G. Schubert, and R. M. Hamwey, "Large-Amplitude Semidiurnal Temperature Variations in the Polar Mesopause: Evidence of a Pseudotide," *Nature* **324**, 347 (1986).
11. J. H. Hecht, R. L. Walterscheid, G. G. Sivjee, A. B. Christensen, and J. B. Pranke, "Observations of Wave-Driven Fluctuations of OH Nightglow Emission From Sondre Stromfjord, Greenland," *J. Geophys. Res.* **92**, 6091 (1987).
12. G. G. Sivjee, R. L. Walterscheid, J. H. Hecht, R. M. Hamwey, G. Schubert, and A. B. Christensen, "Effects of Atmospheric Disturbances on Polar Mesopause Airglow OH Emissions," *J. Geophys. Res.* **92**, 7651 (1987).

13. H-J. Werner, P. Rosmus, and E-A. Reinsch, "Molecular Properties from MCSCF-SCEP Wave Functions. I. Accurate Dipole Moment Functions of OH, OH⁻, and OH⁺," *J. Chem. Phys.* **79**, 905 (1983).
14. S. R. Langhoff, H-J. Werner, and P. Rosmus, "Theoretical Transition Probabilities for the OH Meinel System," *J. Mol. Spectrosc.* **118**, 507 (1986).
15. D. N. Turnbull and R. P. Lowe, "An Empirical Determination of the Dipole Moment Function of OH(X²Π)," *J. Chem. Phys.* **89**, 2763 (1988).
16. F. H. Mies, "Calculated Vibrational Transition Probabilities of OH(X²Π)," *J. Mol. Spec.* **53**, 150 (1974).
17. K. I. Peterson, G. T. Fraser, and W. Klemperer, "Electric Dipole Moment of X²Π OH and OD in Several Vibrational States," *Can. J. Phys.* **62**, 1502 (1984).
18. J. E. Spencer and G. P. Glass, "The Reaction of Atomic Hydrogen with NO₂," *Chem. Phys.* **15**, 35 (1976).
19. J. E. Spencer and G. P. Glass, "The Production and Subsequent Relaxation of Vibrationally Excited OH in the Reaction of Atomic Oxygen with HBr," *Int. J. Chem. Kinet.* **9**, 97 (1977).
20. J. E. Spencer and G. P. Glass, "Some Reactions of OH (v = 1)," *Int. J. Chem. Kinet.* **9**, 111 (1977).
21. G. P. Glass, H. Endo, and B. K. Charurvedi, "Vibrational Energy Transfer from OH to Other Gaseous Hydrides," *J. Chem. Phys.* **77**, 5450 (1982).
22. D. H. Jaffer and I. W. M. Smith, "Time-Resolved Measurements on the Relaxation of OH (v = 1) by NO, NO₂ and O₂," *Faraday Discuss. Chem. Soc.* **67**, 212 (1979).
23. B. D. Cannon, J. S. Robertshaw, I.W.M. Smith, and M. D. Williams, "A Time-Resolved LIF Study of the Kinetics of OH (v = 0) and OH (v = 1) with HCl and HBr," *Chem. Phys. Lett.* **105**, 380 (1984).
24. I. W. M. Smith and M. D. Williams, "Vibrational Relaxation of OH (v = 1) and OD (v = 1) by HNO₃, DNO₃, H₂O, NO, and NO₂," *J. Chem. Soc. Faraday Trans. 2* **81**, 1849 (1985).
25. K. J. Rensberger, J. B. Jeffries, and D. R. Crosley, "Vibrational Relaxation of OH (X²Π, v = 2)," *J. Chem. Phys.*, in press.
26. S. D. Worley, R. N. Coltharp, and A. E. Potter, "Rates of Interaction of Vibrationally Excited Hydroxyl (v = 9) with Diatomic and Small Polyatomic Molecules," *J. Phys. Chem.* **76**, 1511 (1972).
27. G. E. Streit and H. S. Johnston, "Reactions and Quenching of Vibrationally Excited Hydroxyl Radicals," *J. Chem. Phys.* **64**, 95 (1976).
28. B. J. Finlayson-Pitts, D. W. Toohey, and M. J. Ezell, "Kinetics of Interaction of Vibrationally Excited OH (X²Π_i)_{v=9} With Simple Hydrocarbons at Room Temperature," *Int. J. Chem. Kinet.* **15**, 151 (1983).

29. G. D. Greenblatt and J. R. Wiesenfeld, "Time Resolved Emission Studies of Vibrationally Excited Hydroxyl Radicals: OH($X^2\Pi$, $v' = 9$)," *J. Geophys. Res.* **87**, 11145 (1982).
30. R. A. Copeland, J. B. Jeffries, and D. R. Crosley, "Transition Probabilities in OH $A^2\Sigma^+-X^2\Pi_i$ Bands with $v' = 0$ and 1, $v'' = 0$ to 4," *Chem. Phys. Lett.* **138**, 425 (1987).
31. J. A. Coxon and S. C. Foster, "Rotational Analysis of Hydroxyl Vibration-Rotation Emission Bands: Molecular Constants for OH $X^2\Pi$, $6 \leq v \leq 10$," *Can. J. Phys.* **60**, 41 (1982).
32. S. R. Langhoff, E. F. van Dishoeck, R. Wetmore, and A. Dalgarno, "Radiative Lifetimes and Dipole Moments of the $A^2\Sigma^+$, $B^2\Sigma^+$, and $C^2\Sigma^+$ States of OH," *J. Chem. Phys.* **77**, 1379 (1982).
33. P. Felenbok, "Contribution A L'étude du Spectre Moléculaire des Radicaux OH et OD," *Ann. Astrophys.* **26**, 393 (1963).
34. C. Carlone and F. W. Dalby, "Spectrum of the Hydroxyl Radical," *Can. J. Phys.* **47**, 1945 (1969).
35. T. Bergeman, P. Erman, and M. Larsson, "Radiative Properties of the $B^2\Sigma^+$ and $C^2\Sigma^+$ States in OH and OD," *Chem. Phys.* **54**, 55 (1980).
36. R. N. Zare, A. L. Schmeltekopf, W. J. Harrop, and D. L. Albritton, "A Direct Approach for the Reduction of Diatomic Spectra to Molecular Constants for the Construction of RKR Potentials," *J. Mol. Spectros.* **46**, 37 (1973).
37. R. A. Copeland, M. J. Dyer, and D. R. Crosley, "Rotational-Level-Dependent Quenching of $A^2\Sigma^+$ OH and OD," *J. Chem. Phys.* **82**, 4022 (1985).
38. M. H. Alexander, "Rotationally Inelastic Collisions Between a Diatomic Molecule in a $^2\Sigma^+$ Electronic State and a Structureless Target," *J. Chem. Phys.* **76**, 3637 (1982).

APPENDIX A

Laser-Induced Fluorescence of the $B^2\Sigma^+-X^2\Pi_i$ System of OH:
Detection of $v'' = 8$ and 9

Andrew D. Sappey, David R. Crosley, and Richard A. Copeland
Molecular Physics Laboratory
SRI International
Menlo Park, California 94025

ABSTRACT

The previously unobserved $B^2\Sigma^+-X^2\Pi_i$ electronic system of OH is detected by laser-induced fluorescence in a low-pressure flow system. OH is produced in high vibrational levels of the ground electronic state by the $H + O_3$ reaction. Light from a frequency-doubled tunable dye laser excites the radical via the (0,8), (0,9), and (1,8) bands of the $B^2\Sigma^+-X^2\Pi_i$ transition at 225, 236, and 221 nm, respectively. The fluorescence is detected in the $B^2\Sigma^+-A^2\Sigma^+$ system in the visible and near ultraviolet. Measured emission intensities in the (0,3) to (0,9) and the (1,3) to (1,9) bands of B-A are in good agreement with previous theoretical calculations. The experimental branching ratio for emission between the B-A (0,3) and B-X (0,10) bands is about three times larger than theoretically predicted. Detection of high-lying vibrational levels in the electronic ground state, $v'' = 6$ through 15, for experiments in collision dynamics and reaction kinetics, is feasible using the B-X system.

To appear in the Journal of Chemical Physics

MP 88-239R
December 12, 1988

I. INTRODUCTION

The hydroxyl radical is a key intermediate in the chemistry of combustion and of the atmosphere. Its chemical reaction rate constants are often measured in flow or photolysis systems using laser-induced fluorescence (LIF) of the strong bands of the $A^2\Sigma^+ - X^2\Pi_i$ system that originate from the low-lying vibrational levels of the ground electronic state. In situ measurements in flames and other similar practical systems using LIF in these same transitions are commonplace. Amenable to realistic theoretical calculations, OH is also a prototypical molecule for the study of quantum-state-specific collision processes, particularly those providing dynamical information through resolution of spin-orbit and λ -doublet components as well as rotational and vibrational states.

Vibrational distributions in the ground state of OH are difficult to measure for several reasons. The conventional A-X LIF method ($\Delta v = 0$ and $+1$) is limited by rapid predissociation of the A-state vibrational levels ($v' \geq 2$),¹ while infrared emission studies within the ground state are complicated by low sensitivity and a controversy over the relative magnitude of the vibrational band transition strengths.² Recently, LIF using off-diagonal bands ($\Delta v \leq -1$) in the A-X system have characterized the vibrational distribution up to $v' = 3$ for the $O(^1D) + H_2$ reaction³ and the relative magnitude of these weak bands have been measured.⁴ In the later work, LIF bands were observed that have oscillator strengths as much as a factor of 10^5 smaller than the strong (0,0) band.⁴ However, with powerful lasers which can saturate even very weak transitions, such small oscillator strengths pose little limitation on detection via off-diagonal vibrational bands. Therefore, the A-X system is suitable for detection of ground state vibrational levels up through $v = 5$ and perhaps 6.⁴ Thus far, higher levels have only been detected by infrared and visible emission within the ground state in the Meinel bands.⁵

An alternative method to measure the collision dynamics of yet higher vibrational levels within the ground state, reaction product distributions, and the levels populated as a result of collisional quenching of the A state is needed. Prominent among these needs are investigations of the kinetics of Meinel band emission from the upper atmosphere, which is the major constituent of the airglow in the near infrared.⁵ This emission is used as a diagnostic tool for measuring the temperature and understanding the chemistry ~100 km above the earth's surface, and forms an undesirable background for infrared remote sensing. Meinel band emission results from the atmospheric production of OH in levels up to $v = 9$ through the $H + O_3$ reaction.⁶ Radiative and collisional relaxation of the very high levels occurs giving rise to strong light in the visible (through multiquantum transitions, $|\Delta v| = 4, 5, \text{ and } 6$) and near infrared. Vibrational energy transfer resulting from collisions with O_2 , N_2 , O_3 , and O is important in determining the emission distribution, but rate constants for this process are poorly known.⁷

We have observed laser-induced fluorescence in a new electronic band system of OH, $B^2\Sigma^+ - X^2\Pi_i$. The B state has a much larger internuclear equilibrium distance than the X state, and the wavefunctions of its two bound vibrational levels overlap those of high-lying vibrational levels in X. It is therefore quite suitable for detection of OH in these high levels. The high vibrational levels in X are prepared by the $H + O_3$ reaction in a low-pressure flow cell,⁶ and laser excitation occurs in the ultraviolet, to populate $v = 0$ and 1 of B. Fluorescence to the A state is detected. Here, overlap is again with high lying vibrational levels, and we observe emission to $v = 3$ through 9 (the last bound level) of A. In this paper, we present relative transition probabilities for several B-A bands and compare them with previous theoretical and experimental values. The ratio of oscillator strengths of the B-X and B-A systems is also obtained. In a subsequent paper,⁸ we will describe fluorescence lifetime determinations and collisional dynamics for various rotational levels of $v' = 0$ and 1 in $B^2\Sigma^+$.

The spectroscopy of the B state has been studied by dispersing B-A emission from discharges in water vapor.^{9,10} The B-state potential curve is very shallow with a dissociation energy of about 1350 cm^{-1} and a large r_e of 2.05 \AA , twice that of the A or X states. The A state is well studied and possesses ten bound levels. Previous experimental data on the relative intensity of the (0,6), (0,7), and (0,8) bands are available from emission studies of Felenbok⁹ and Bergeman, Erman and Larsson (BEL).¹¹ In both studies, Franck-Condon factors $q_{v'v''}$ and r-centroids were calculated for the B-A system, and the r-centroid approximation was used to describe the intensity measurements. The electronic transition moment, $R_e(r)$, was observed to decrease with increasing internuclear distance r in the range covered by these bands (1.7 to 2.0 \AA); this transition is forbidden in the separated atom limit.

More recently, Langhoff et al.¹² performed a theoretical study of the X, A, B, and C states of OH. For each electronic system, they calculate an ab initio transition dipole moment as a function of r , and use it to compute transition probabilities in conjunction with empirical potentials for all the bands in the B-A and B-X systems. Their results are in good agreement with our measured transition probabilities for the (0,3) to (0,9) and (1,3) to (1,9) sequences in B-A, and agree to within a factor of three for the ratio of intensities for the weak B-A (0,3) and B-X (0,10) bands. Therefore, transition probabilities in these two systems are satisfactorily understood. We conclude, based on these experiments and the theoretical calculations of Langhoff et al.¹² that there is sufficient oscillator strength at wavelengths accessible to lasers to probe, in the X state, $v'' = 6$ through 15. This will open these high vibrational levels of the OH radical to direct study using the sensitive and selective LIF technique, and facilitate many new dynamics and kinetics experiments on this important species.

II. Experimental Details

Vibrationally excited OH radicals are produced via the reaction of hydrogen atoms and ozone in a fast flow reactor. Typically, 0.05 to 0.06 slm (standard liters per minute) of H₂ seeded in a flow of 1.5-3.0 slm of He or Ar is discharged at 2450 MHz to produce H atoms for the reaction. The ozone is prepared using a commercial ozonizer and stored on silica gel at about 200 K. It is injected into the viewing region of the reactor by flowing a small amount of buffer gas through the ozone trap to a gas port on the cell. The amount of buffer gas flow through the trap is adjusted empirically to maximize signal. As the amount of ozone on the trap decreases we must increase the buffer gas flow. Typically, 0.010-0.080 slm of He or Ar flow is needed. The concentration of ozone in the cell is not monitored. The total cell pressure can be varied from approximately 200 mTorr to 10 Torr.

Visible chemiluminescent Meinel band emission from the reaction is bright and facilitates alignment of the detection optics and maximization of hot OH production. OH is excited to the B state using frequency doubled laser light at wavelengths ranging from 221 to 236 nm. This light is produced by frequency doubling in a β -barium borate crystal the output of an excimer-pumped dye laser system. The typical laser energy used is between 0.2 and 1 mJ at 50 Hz. The fundamental and second harmonic are separated by a Pellin-Brocha prism which is manually adjusted to maintain pointing stability as the wavelength is varied.

The fluorescence is collected at right angles and is imaged onto the slit of a 0.35 m monochromator by a two lens collection system. The collimating lens is a 5 cm biconvex focal length quartz lens located approximately 5 cm from the reaction zone. The focusing lens is a 12.5 cm biconvex quartz lens located approximately its focal length from the monochromator slit. A filter (Schott, WG360, 3 mm) blocks laser scatter and prevents its detection through the monochromator in second order. The bandwidth of the

monochromator for all measurements described here is 40 Å. The signal from the EMI 9558Q photomultiplier is amplified and captured in a boxcar integrator with a gate of ~150 ns set to encompass the entire signal. The single shot output of the boxcar is digitized and summed in a lab computer.

Light is also imaged using a one lens collection system onto a Hamamatsu R105 filtered photomultiplier tube to provide an accurate normalization measurement to account for drift in OH density, laser amplitude or frequency during fluorescence scans. Spectral filters in this channel allow the total fluorescence signal from a single B-A vibrational band to be detected while discriminating against scattered laser light and discharge light. When exciting the $B^2\Sigma^+ v' = 0$ level, two colored glass filters (Schott GG495 and GG455, both 3 mm) and an interference filter (Corion, LS-550) are used to detect the (0,7) band. For the $B^2\Sigma^+ v' = 1$ level, three filters (Schott OG 530 and OG 550, both 3 mm and Corion LS-600) are used to detect the (1,9) band. Discharge light is further discriminated against by aperturing this photomultiplier tube with ~6 mm slits aligned along the laser beam axis. We estimate that the normalization signal for (0,7) contains less than 0.1% scattered light. The output is integrated directly by a second boxcar without prior amplification, then digitized and stored in the same manner as the signal.

III. Results

Figure 1 depicts a portion of the B-X (0,8) band excitation spectrum, taken with the integrator gate set to encompass the entire fluorescence decay. The individual rotational branches are readily assigned, using a spectral simulation program¹³ and the spectroscopic constants of the B state^{9,10} and high lying vibrational levels of the X state.¹⁴

The rotational temperature of $v = 8$ in OH X, based on the spectral intensities of Figure 1, is far colder than the expected 300 K. In the earlier work of BEL, a similar effect was observed in B-A emission spectra: the rotational temperature of the B state based on the intensities of rotational lines from $N' = 0-5$ was 120 K. This was attributed to a cold nascent distribution following dissociation of H_2O by the 20 keV electrons used to produce OH in that experiment. However, we believe it is caused by a fluorescence yield that depends upon rotational level, due to predissociation of the B state in this region. Measurements of the time dependence of the fluorescence decay constant⁸ show that the lifetime of rotational levels in both $v' = 0$ and 1 decreases about a factor of three as N' is increased from 0 to 2 for the F_1 levels. From a preliminary analysis, we find fluorescence lifetimes less than 150 ns. Excitation spectra obtained with a narrow, 10 ns gate placed on the leading edge of the fluorescence pulse measure the initial amplitude of the signal, and are less affected by the quantum yield variation due to N' -dependent predissociation. These give sensible temperatures near 300 K. Understanding this predissociation is extremely important for accurate measurement of individual rotational populations in high lying vibrational levels of the ground state using B-X LIF, and will be discussed in the subsequent paper.⁸

Figure 2 shows the $B^2\Sigma^+-A^2\Pi_i$ fluorescence spectra obtained by exciting the unresolved $Q_1(1)$ and $Q_{P21}(1)$ feature (labeled $Q_1(1)$ throughout) of the B-X (0,8) and (1,8) bands. As expected from a simple picture of the B and A vibrational overlap, fluorescence from $v' = 0$ shows a smooth variation while that from $v' = 1$ exhibits a single minimum, which occurs near the (1,8) band. An abrupt cutoff of the envelopes to the red is seen in the scan in Fig. 2(b) in the position where the (1,10) band would be; this occurs because the $v = 10$ would lie above the dissociation limit of the A state. In addition, there is some evidence for $v' = 1$ to 0 vibrational transfer within the B state while pumping the (1,8) band; note the small, but reproducible, signal just on the long wavelength side of the

(1,6) and (1,7) bands. At the 5 Torr total pressure used for this scan, a reasonable vibrational transfer rate coefficient ($\sim 5 \times 10^{-12} \text{ cm}^3 \text{ s}^{-1}$) would account for these small bands.

Fluorescence scans such as those in Fig. 2 are used to determine the band transition probabilities. Most of the dispersed fluorescence spectra are obtained using this $Q_1(1)$ feature for excitation. In a check for possible rotational effects, we also excite $v' = 1$ via the $R_1(3)$ and $R_{Q_2}(3)$ feature. No differences are observed. The raw data are normalized by the total signal intensity, and the spectral response of the detection system is determined using calibrated standard deuterium and tungsten lamps.

Relative transition intensities for the bands illustrated in Fig. 2 are listed in Table I, given as the fractional contribution of each band to the total emission strength of $v' = 0$ and 1. The values are averaged over seven independent experiments for the $v' = 0$ bands and six for the $v' = 1$ bands. The reported errors are two standard deviations of the unweighted mean. The error bars are typically 10% of the reported values, which is a good reflection of our ability to measure the band intensities given the inherent uncertainties of the experiment.

In Fig. 3 we show a fluorescence spectrum in the region of the B-X (0,10) and B-A (0,3) bands obtained by exciting via $Q_1(1)$ feature of the B-X (0,8) band. From this data we can extract the first experimental information on the relative strength of the B-A and B-X transitions. Three independent scans are taken to obtain an average, weighted by signal to noise ratio (which is low due to the small transition probabilities and diminished monochromator response at these wavelengths). The result¹⁵ is a ratio $I[\text{B-A (0,3)}]/I[\text{B-X (0,10)}] = 1.6 \pm 0.5$, where the error represents the range of values obtained. A measurement of the ratio of the two observed bands of the B-X system is also made. The

result is $I(0,9)/I(0,10) = 2.0 \pm 1.0$, where again low signal levels are responsible for the large error.

Additionally, we observe an emission signal from the (0,0) band of the A-X system. Although clearly induced by the laser, the signal is not resonant with excitation of individual vibrational/rotational levels of the B state of OH. The time dependence of the signal indicates that the emitting state, $v = 0$ of A, is not formed promptly by the laser pulse but follows it at a time indicative of chemical reaction. Fluorescence is not observed from higher vibrational levels of the A state. We tentatively ascribe this fluorescence to a chemiluminescent reaction between H atoms present in the flow cell with $O(^1D)$ produced by photodissociation of O_3 , although the absence of emission from higher vibrational levels is puzzling.

At these laser wavelengths, O_3 is dissociated with high quantum yield to form $O(^1D)$ and $O_2(^1\Delta)$.¹⁵ Production of $OH(A)$ by the reactions of $O(^1D)$ with H_2 and H_2O impurity, or by $O_2(^1\Delta) + H$, can be ruled out on the basis of energetics. However, the reaction $O(^1D) + H + M \rightarrow OH(A) + M$ is exothermic by $\sim 55 \text{ kcal mol}^{-1}$, enough to populate many vibrational levels of $OH(A)$. $O(^3P)$, which could be formed¹⁵ by quenching or the reaction of $O_2(^1\Delta)$, could react with H atoms either via the reaction $O(^3P) + H + M \rightarrow OH(A) + M$ (exoergic by $9.7 \text{ kcal mol}^{-1}$) or by inverse predissociation. The first possibility has just enough energy to populate $OH(A) v' = 1$, and the inverse predissociation would preferentially populate high N' in $v = 1$ and all N' in $v = 2$ since these vibrational levels are in the vicinity of the crossing between the $A^2\Sigma^+$ and $a^4\Sigma^-$ states. Thus, for each possible mechanism, we would expect to see emission from vibrational levels higher than $v = 0$ in $OH(A)$. Additional experimental studies are necessary to provide a conclusive mechanism for this chemiluminescent signal.

IV. Discussion

Table 1 presents the experimental values of the band strengths, listed as the fractional contribution of the intensity of each observable vibrational band to the total. These are compared with theoretical values calculated by Langhoff et al.,¹² tabulated here in the same way. Langhoff et al.¹² performed configuration interaction calculations employing three different basis sets. The largest set, labeled by them as I, appears to provide the most accurate potentials for the A, B, and X state, although there is some deviation from Klein-Dunham curves⁸ for the high vibrational levels of A and X that are of interest here. They then computed transition probabilities for individual vibrational bands of the B-A and B-X systems using ab initio electronic transition moments and vibrational wavefunctions. The error quoted by Langhoff et al.¹² for calculated radiative lifetimes of the B state is 20%.

The theoretical and experimental results are in good agreement. Most of the band strengths agree within ten percent, less than the experimental error and well less than the combined precision of such an experiment and the expected uncertainty in the calculation. There is a larger discrepancy for the (0,8) and (0,9) bands; however the experiment and theory only differ by only 16 and 32%, respectively. At these vibrational levels in the A state there is disagreement between the calculated ab initio potential surfaces and the empirical Klein-Dunham potentials derived from spectroscopic constants (see Fig. 1, Ref. 12). Such a complication would be expected to also affect the (1,8) and (1,9) bands; however, these values agree remarkably well.

We also compare the intensities of selected bands with those obtained from emission studies. Both Felenbok⁹ and BEL¹¹ measure relative intensities of the three strongest bands emitted by $v = 0$: (0,6), (0,7), and (0,8). In both papers, these intensities are represented only as points on a plot of the electronic transition moment as a function of

internuclear distance, invoking an r-centroid approximation and reducing the experimental data using their own calculated Franck-Condon factors. We have retrieved the experimental intensities by computing $I_{v'v''} \propto q_{v'v''}^3 |R_e(r_{v'v''})|^2$. The R_e values are taken from Fig. 19 of Ref. 9 and Fig. 6 of Ref. 11, and the $q_{v'v''}$ from the tables in each paper. The results are normalized to the total intensity in these three bands, and listed in Table II along with our experimental results and those of Langhoff et al.¹² The agreement among our results and those of BEL is good, well within expected accuracies (error bars on the BEL plot are 20 to 30%). The BEL value for (0,8) lies midway between our experimental value and the theoretical calculation and does not resolve the differences described above. Felenbok's results differ slightly, primarily because the (0,6) band looks too large compared with (0,7) when compared to the other data.

The B-X system is much weaker than the B-A, as evidenced by the comparable intensities of the (0,10) band of the former, one of the stronger in B-X, and the very weak (0,3) band of B-A (see Fig. 3 and Table I). The total emission transition probability into all vibrational levels is computed¹² to be about a factor of 17 higher for B-A compared to B-X, but in the latter system the transitions are spread over a larger number of bands, so that a strong B-X band is about a hundredfold weaker than a strong B-A band. The comparison of theory and experiment remains good, well within experimental error, for the measurements involving bands of B-X. The experimental ratio for $I(0,9)/I(0,10)$ in B-X is 2.0 ± 1.0 , compared to the theoretical value of 2.3. The ratio of total system oscillator strengths is contained in the ratio $I[\text{B-A } (0,3)]/I[\text{B-X } (0,10)]$, for which the experimental determination is 1.6 ± 0.5 and the theoretical result is 0.5. The theoretical results for the latter ratio differ from experimental values by more than the error bars. This is possibly due to the difficulty of calculating a realistic empirical potential for high vibrational levels ($v \geq 10$) of OH, $X^2\Pi_i$ (see Fig. 1, Ref. 12) and the proximity of the electronic transition moment of B-X to its zero crossing in this region. Calculations of these weak transitions

are difficult and involve the relative magnitude of two different electronic transition moments.

These results show that the theoretical calculations of Langhoff et al.¹² form good representations of the band transition probabilities in the $B^2\Sigma^+-A^2\Sigma^+$ electronic system, and that, within a factor of about 3, the ratio of oscillator strengths for the B-A and B-X systems. In Table III, we compile, for bands of the B-X system, values of the wavelength λ and the Einstein absorption coefficient B, taken from the theoretical results of Langhoff et al.¹² for the Einstein emission coefficient A for each band. This table can be used to determine the feasibility of measuring other vibrational levels. To gauge its size, the B value for the (0,0) band of the A-X system, used routinely for OH measurements, is also given, as is the value for the highly off-diagonal (1,4) band, which has been employed to detect OH in $v = 4$ of the ground state in a dynamics experiment.¹⁶

The absolute absorption coefficient also includes the absolute radiative rate. This quantity remains in dispute, with experimental values for $B^2\Sigma^+$ decay times of ~ 100 ns⁸ and $2 \mu s$,¹¹ and a computed radiative lifetime¹² of ~ 300 ns. Nonetheless, the strong signals observed for the (0,8) band indicate easy detection of at least $v = 7$ through 11 in the ground state. Above $v = 11$, the absorption coefficients in both $v' = 0$ and 1 oscillate up and down due to the electronic transition moment crossing zero in this region and becoming negative. The magnitudes of these transitions will be extremely sensitive to the transition moment in this region. However, from the results in Table III, the detection of vibrational levels up to $v = 15$ appears feasible. The oscillator strengths for $v = 5$ and 6 are strong enough for facile measurement, although the laser wavelengths must be generated with Raman shifting, not direct frequency doubling. Combined with the ability to monitor up through $v = 5$ or 6 via A-X excitation, we can now study collision dynamics, reaction kinetics, and photochemical and reactive product distributions for the range of vibrational levels from $v = 0$ to 15 in the important OH molecule.

V. Acknowledgement

This work was sponsored by the Air Force Geophysics Laboratory under contract No. F19628-87-K-0043, AFOSR task 2310G4.

References

1. J. Brzozowski, P. Erman, and M. Lyyra, Phys. Scr. 17, 507 (1978).
2. D. N. Turnbull and R. P. Lowe, J. Chem. Phys. 89, 2763 (1988).
3. C. B. Cleveland, G. M. Jursich, M. Troler, and J. R. Wiesenfeld, J. Chem. Phys. 86, 3253 (1987).
4. R. A. Copeland, J. B. Jeffries, and D. R. Crosley, Chem. Phys. Lett. 138, 425 (1987).
5. A. B. Meinel, Astrophys. J. 111, 555 (1950).
6. D. Klenerman and I.W.M. Smith, J. Chem. Soc. Faraday Trans. 2 83, 229 (1987).
7. I. C. McDade and E. J. Llewellyn, J. Geophys. Res. 92, 7643 (1987).
8. A. D. Sappey, D. R. Crosley, and R. A. Copeland, in preparation.
9. P. Felenbok, Ann. Astrophys. 26, 393 (1963).
10. C. Carlone and F. W. Dalby, Can. J. Phys. 47, 1945 (1969).
11. T. Bergeman, P. Erman, and M. Larsson, Chem. Phys. 54, 55 (1980).

12. S. R. Langhoff, E. F. van Dishoeck, R. Wetmore, and A. Dalgarno, *J. Chem. Phys.* 77, 1379 (1982).
13. R. N. Zare, A. L. Schmeltekopf, W. J. Harrop, D. L. Albritton, *J. Mol. Spectros.* 46, 37 (1973).
14. J. A. Coxon and S. C. Foster, *Can J. Phys.* 60, 41 (1982).
15. H. Okabe, *Photochemistry of Small Molecules* (John Wiley and Sons, New York, 1978), p. 237-246.
16. D. R. Crosley and R. A. Copeland, in *Laser Applications to Chemical Dynamics*, M. A. El-Sayed, ed., *Proceedings of the Society of Photo-Optical Instrumentation Engineers* 742, 6 (1987).

Table 1. Comparison of experimental and ab initio relative B-A transition strengths.

B-A	(0,3)	(0,4)	(0,5)	(0,6)	(0,7)	(0,8)	(0,9)
exp.	0.0029 (0.0006) ^b	0.019 (0.001)	0.09 (0.01)	0.24 (0.01)	0.393 (0.006)	0.250 (0.006)	0.0056 (0.0008)
theory ^a	0.0030	0.021	0.092	0.26	0.41	0.21	0.0038
B-A	(1,3)	(1,4)	(1,5)	(1,6)	(1,7)	(1,8)	(1,9)
exp.	0.011 (0.002)	0.051 (0.006)	0.18 (0.01)	0.295 (0.006)	0.151 (0.006)	0.034 (0.006)	0.28 (0.01)
theory	0.0090	0.051	0.17	0.32	0.16	0.034	0.26

^aResults of calculations of Ref. 12. Values for each vibrational level are independently normalized to one.

^bThe values in parentheses below the experimental value is the 2- σ estimated error as described in the text.

Table 2. Relative B-A transition probabilities in $v' = 0$, normalized to the sum of the (0,6), (0,7), and (0,8) vibrational bands.

Band	Present Results	Felenbok Ref. 9	BEL Ref. 11	Langhoff et al. Ref. 12
(0,6)	0.27	0.37	0.29	0.30
(0,7)	0.45	0.39	0.46	0.47
(0,8)	0.28	0.23	0.25	0.23

Table 3. Approximate wavelengths and relative absorption strengths of various electronic transitions in the OH radical.

B-X	(0,5)	(0,6)	(0,7)	(0,8)	(0,9)	(0,10)
B ^a	9.7(3)	3.1(4)	7.3(4)	1.1(5)	1.1(5)	6.0(4)
λ^b	192	202	213	225	237	249
	(0,11)	(0,12)	(0,13)	(0,14)	(0,15)	
B	9.3(3)	9.3(2)	4.7(3)	1.5(3)	2.2(1)	
λ	261	274	286	298	310	
	(1,5)	(1,6)	(1,7)	(1,8)	(1,9)	(1,10)
B	1.6(4)	4.3(4)	8.3(4)	1.0(5)	7.0(4)	1.8(4)
λ	189	200	210	222	233	245
	(1,11)	(1,12)	(1,13)	(1,14)	(1,15)	
B	3.3(1)	7.7(2)	2.6(3)	2.2(4)	2.2(3)	
λ	257	269	281	292	304	
A-X	(0,0)	(1,4)				
B ^c	8.3(6)	1.4(3)				
λ	308	452				

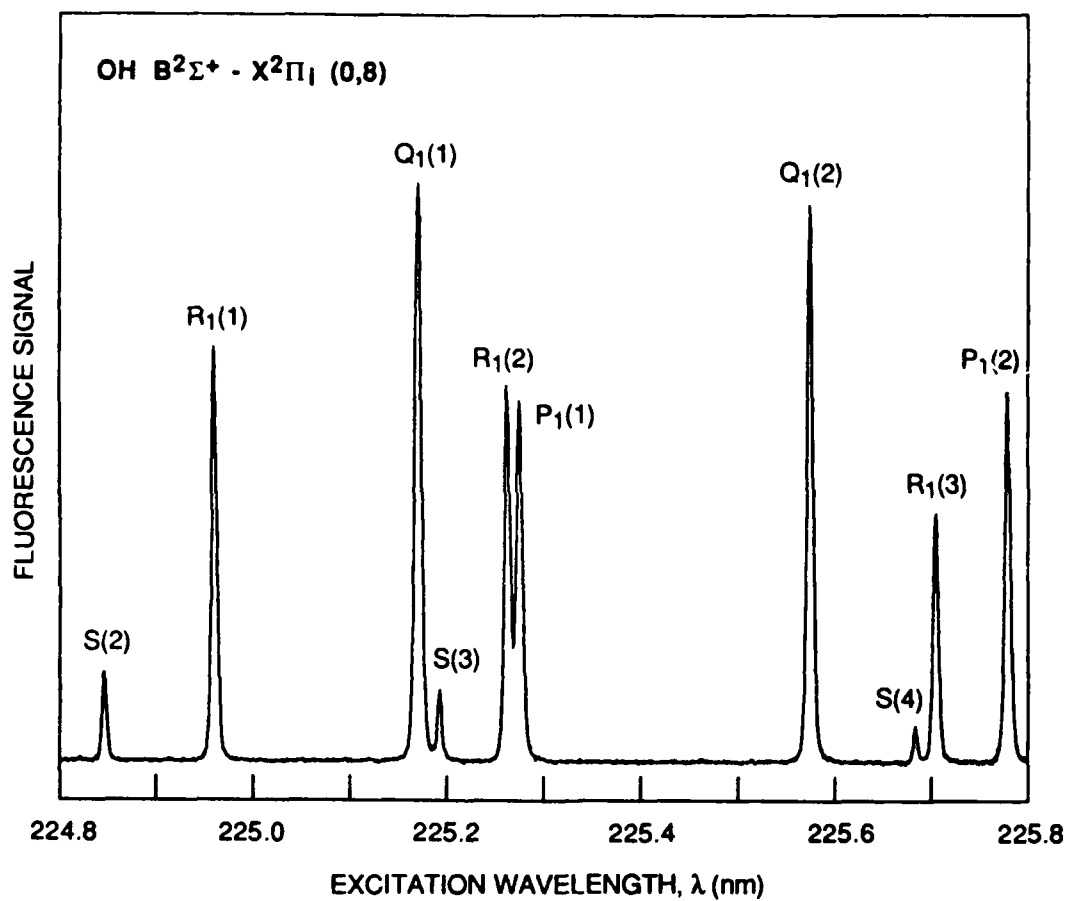
^aUnits of $\text{cm}^2 \text{erg}^{-1} \text{s}^{-1}$. Calculated from the A values of Ref. 12. Values in parentheses are the exponent.

^bUnits of nm. Calculated from Ref. 10.

^cCalculated from the A values of Ref. 4.

Figure Captions

- Figure 1. Excitation scan of the OH $B^2\Sigma^+-X^2\Pi_i$ (0,8) band. Plotted is the B-A (0,7) band fluorescence signal vs. uncorrected dye laser dial reading. The branches are unambiguously assigned based on a spectral simulation using the constants of Ref. 13. The wavelength scale is uncertain by at most 0.04 nm ($\sim 10 \text{ cm}^{-1}$).
- Figure 2. Dispersed fluorescence scan corrected for detection system response of the $B^2\Sigma^+-A^2\Pi_i$ system. The top trace (a) is obtained by exciting the $Q_1(1)$ and QP_{21} feature of the (0,8) B-X system. The fluorescence connects the B state $v' = 0$ to the A state, $v'' = 3-9$. The bottom trace (b) is obtained by exciting the $Q_1(1)$ and QP_{21} feature of the (1,8) B X system. The fluorescence connects the B state $v' = 1$ level to the A state levels, $v'' = 3-9$.
- Figure 3. Dispersed fluorescence scan demonstrating the branching of fluorescence between the B-A and B-X systems. The figure is uncorrected for detection response. After such correction, the ratio $I[B-A (0,3)]/I[B-X (0,10)]$ is 1.6 ± 0.5 . The spectrum is obtained by pumping the $B^2\Sigma^+-X^2\Pi_i$ (0,8) $Q_1(1)$ and QP_{21} overlapped feature.



RA-330583-171

FIGURE 1

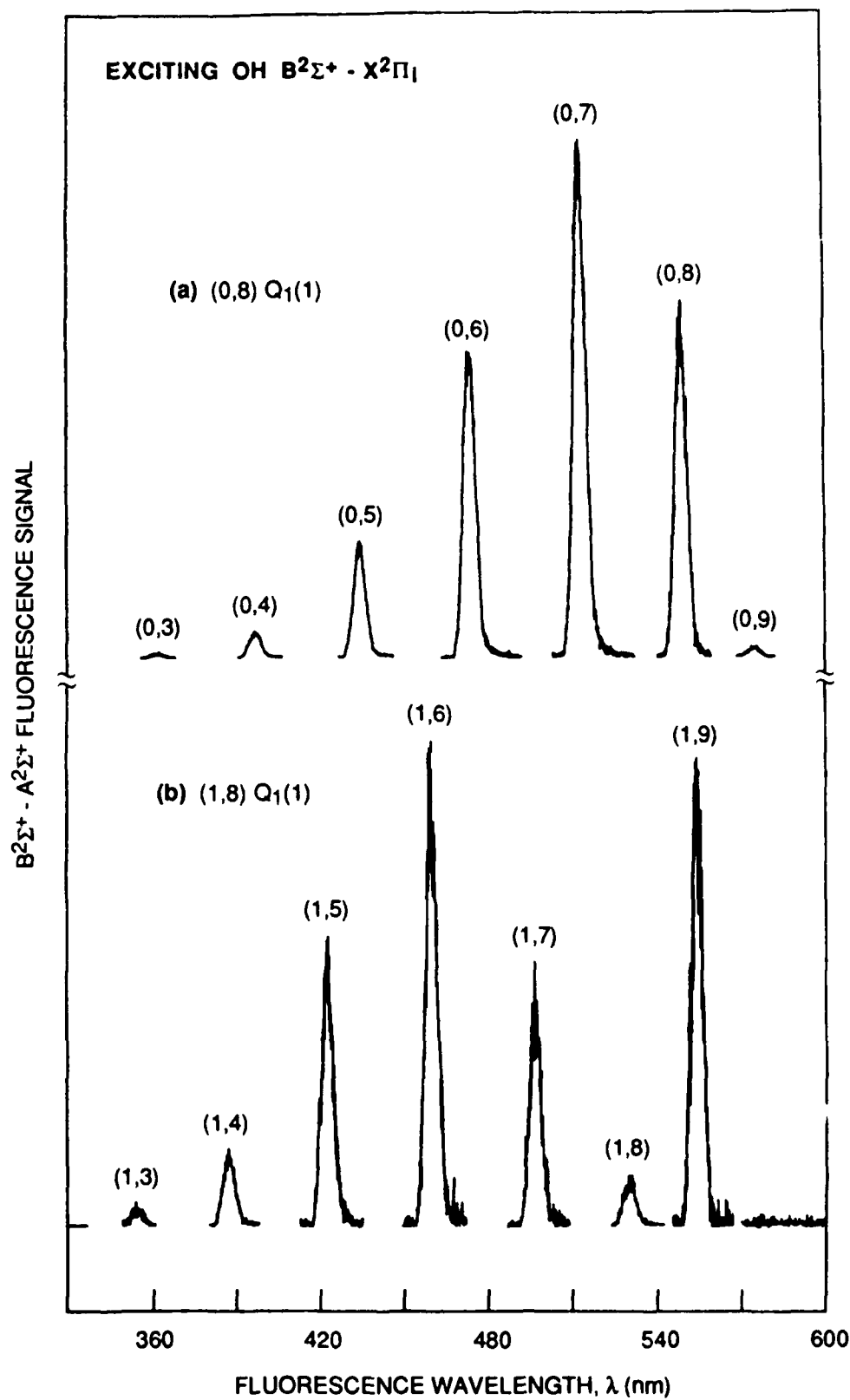
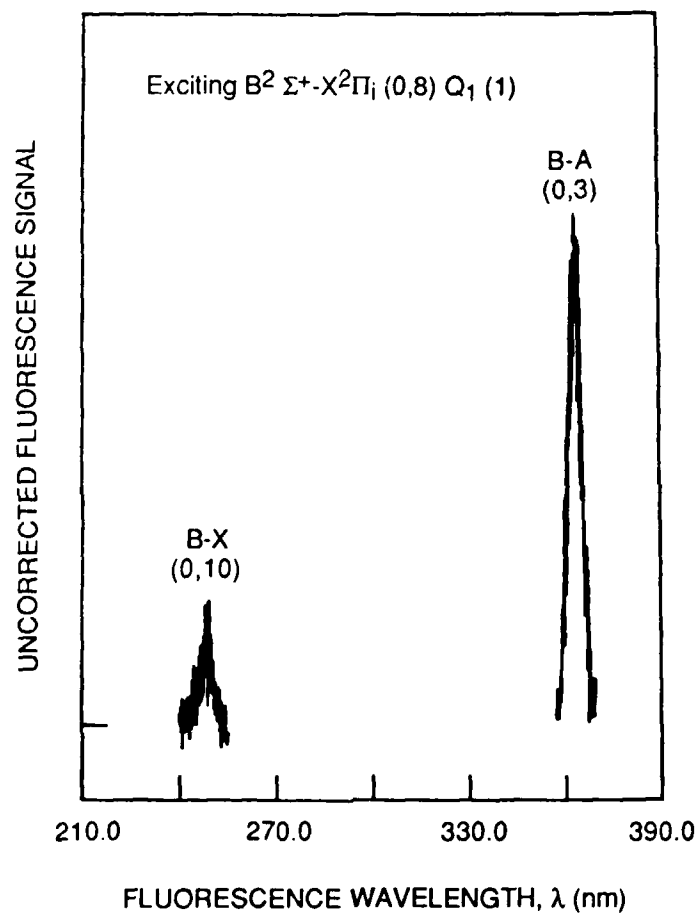


FIGURE 2

RA-330583-172



RA-3772-5

FIGURE 3

APPENDIX B

LASER-INDUCED FLUORESCENCE IN THE $B^2\Sigma^+-X^2\Pi_i$ SYSTEM OF OH

Andrew D. Sappey, David R. Crosley and Richard A. Copeland
Molecular Physics Laboratory, SRI International
Menlo Park, California 94025

ABSTRACT

Laser-induced fluorescence in the previously unobserved B-X system is used to detect the high vibrational levels of ground state OH generated by the reaction of H and O_3 . Light (220-240 nm) from a frequency-doubled tunable dye laser excites the (0,8), (0,9) and (1,8) vibrational bands of the B-X system. The B state then fluoresces predominantly to the $A^2\Sigma^+$ state between 400 and 600 nm. Weaker fluorescence to the X state is also observed. From the temporal evolution of the fluorescence, lifetimes are extracted for different vibrational, rotational, and fine-structure levels of the B state. Large variations are observed between these levels indicating an unexpected predissociation.

INTRODUCTION AND EXPERIMENTAL APPROACH

High vibrational levels of the OH radical ($X^2\Pi_i$, $v'' \leq 9$) are produced in the earth's upper atmosphere by the reaction of H and O_3 . These highly excited molecules then fluoresce via vibrational transitions within the ground state giving rise to visible and near-infrared light. This emission is used as a diagnostic for upper atmosphere temperature, concentrations, and dynamics. Models of this emission require as input absolute vibrational band transition strengths and rotational and vibrational energy transfer rate constants and mechanisms. A sensitive and state selective method of probing high vibrational levels in OH is required to characterize these collisional energy transfer processes. In this work, we describe the development of such a method, B-X laser-induced fluorescence (LIF).

The OH radicals are produced in $v'' \leq 9$ in a microwave-discharge flow cell by the reaction of H with O_3 and excited to the $B^2\Sigma^+$ state by light between 220 to 240 nm (~ 1 mJ) from a frequency-doubled excimer-pumped dye laser. The total cell pressure can be varied from 0.2 to 2 Torr with helium as the major component. The LIF is monitored by a filtered photomultiplier and also dispersed by a monochromator. The signals are amplified and detected with either a boxcar integrator or a 100 megasample s^{-1} transient digitizer. A complete description of the experimental approach can be found in Ref. 1.

DISPERSED FLUORESCENCE RESULTS

We have measured the intensity of the dispersed fluorescence from both $v' = 0$ and 1 of the B state following excitation of the overlapped $Q_1(1)$ and Q_{P21} rotational feature.¹ We observe fluorescence to levels $3 \leq v \leq 9$ of $A^2\Sigma^+$ between 350 and 600 nm. The three strongest vibrational bands from $v' = 0$ are (0,7), (0,8) and (0,6) at 510, 550, and 470 nm, while those from $v' = 1$ are (1,6), (1,9) and (1,5) at 460, 555, and 420 nm. These bands lie at significantly longer wavelengths than the excitation laser so scattered laser light is not a problem in the LIF detection. The fluorescence cuts off abruptly to the red of the (0,9) and (1,9) B-A bands, because $v = 10$ of the A state is not bound. The expected minimum in the fluorescence pattern from $v' = 1$

occurs in the vicinity of the (1,8) band. The relative vibrational band transition probabilities for the B-A bands agree very well with recent theoretical calculations by Langhoff et al.²

In the ultraviolet we detect small signals that result from fluorescence in the (0,9) and (0,10) bands of the B-X electronic system.¹ These bands are similar in intensity to the weakest bands of the B-A system and we find that $I[B-A(0,3)]/I[B-X(0,10)] = 1.6 \pm 0.5$; about 0.3% of the B-A fluorescence occurs in the (0,3) band. The theoretical result² for the above ratio is 0.5 which differs from the experimental result by about a factor of three.

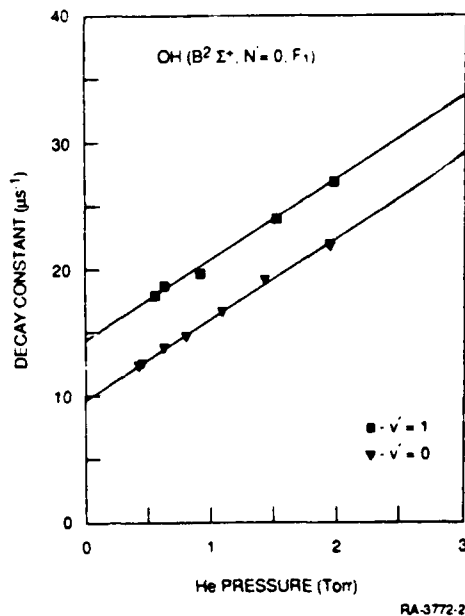


Figure 1

FLUORESCENCE LIFETIMES OF THE B STATE

Fluorescence lifetimes for the B state are obtained from the zero pressure intercept of a plot of the fluorescence decay constant versus the He pressure as shown in Figure 1. We fit the time-dependent fluorescence signals from 90 to 10% of the peak value to a single exponential to obtain the decay constants. In Fig. 1, the boxes are data taken exciting $v' = 0$, $N' = 0$, $J' = 0.5$ while the triangles are taken exciting the same rotational state in $v' = 1$. The lines are the best linear least squares fit to the data. Note the larger zero pressure intercept for $v' = 1$ indicating a longer fluorescence lifetime, τ for $v' = 0$. The characteristic slope of each line is due to collisional removal of the excited rotational level and will be discussed in detail in a future publication. We have made zero pressure lifetime measurements for the F_1 and F_2 spin components of rotational levels,

$N = 0, 1$, and 2 in $v' = 0$, and 1 of the B state. The results are presented in Figure 2 where we have chosen to plot the lifetimes versus the total angular momentum J . The data for the F_1 components are obtained by exciting to only the F_1 level, while the points for F_2 are extracted from data in which a mixture of F_1 and F_2 fine-structure levels are populated. We estimate an experimental uncertainty of in the fluorescence lifetimes of $\pm 15\%$ for the F_1 levels and $\pm 50\%$ for the F_2 levels.

The significant variation of τ with N , v , F_1 and F_2 seen in Fig. 2 signals a predissociation in the B state. (Note that the lifetime of the F_1 component of rotational level $N-1$ is nearly equal to that of the F_2 component of level N .) This conclusion is supported by a calculated radiative lifetime² of ~ 300 ns for $v = 0$ and ~ 510 ns for $v = 1$, which is much longer than we observe in the experiments. Our lifetimes are over an order of magnitude shorter than obtained by previous indirect measurements³ and, coupled with the theoretical results,² indicate that the B fluorescence lifetimes of Ref. 3 are in error. Although we can not definitively assign the predissociation based on our limited data, several points can be made with certainty. First, the magnitude of our values (20-100 ns) indicates that the predissociation is weak. A weak predissociation may be due to second order effects (especially spin-orbit) in the electronic matrix element, or small vibrational overlap factors resulting from non-crossing curves.⁴ Second, the lifetimes for the F_1 levels in both $v' = 0$, and 1 decrease as J increases

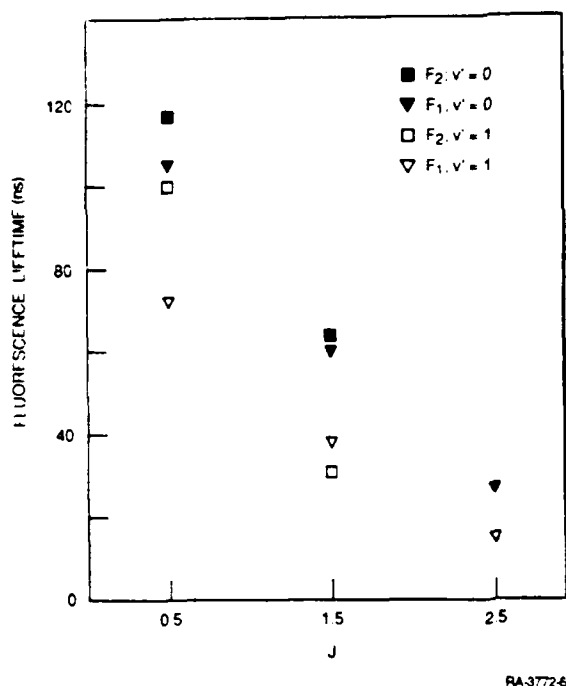


Figure 2

(Fig. 2). This type of behavior is characteristic of rotational and gyroscopic predissociations.⁴ Rotational predissociation can be eliminated because we are observing levels well below the dissociation limit of the B state. The predissociation observed here is therefore distinct from the rotational predissociation of higher rotational levels of the B state discussed by Felenbok.⁵

On a more speculative level, further information is gained from consideration of possible perturbing states that could induce a gyroscopic predissociation ($\Delta\Lambda\pm 1$, $\Delta S=0$). The lower lying asymptote, $O(^1D) + H(^2S)$, gives rise to three doublet states, $2\Sigma^+$, 2Π , and 2Δ . The first of these constitutes the well-known $A^2\Sigma^+$ state. Of the remaining states, only the 2Π state is capable of predissociating the $B^2\Sigma^+$ state through first order effects.

Calculations show a crossing (barely) between the $B^2\Sigma^+$ and repulsive 2Π states on the inner limb; this is the only curve which appears to cross the B state.⁶ However, the $2\Sigma^+-2\Pi$ gyroscopic interaction should be strong. The weakness of the observed interaction suggests that the curves may not actually cross, or that another predissociation mechanism is occurring. Further experiments investigating predissociation in OD and in higher rotational levels should unambiguously characterize this predissociation.

ACKNOWLEDGMENT

This work was sponsored by the Air Force Geophysics Laboratory under contract No. F19628-87-K-0043, AFOSR task 231064.

REFERENCES

1. A. D. Sappey, D. R. Crosley and R. A. Copeland, J. Chem. Phys., in press (1989).
2. S. R. Langhoff, E. F. van Dishoeck, R. Wetmore and A. Dalgarno, J. Chem. Phys. **77**, 1379 (1982).
3. T. Bergeman, P. Erman and M. Larsson, Chem. Phys. **54**, 55 (1980).
4. H. Lefebvre-Brion and R. W. Field, Perturbations in the Spectra of Diatomic Molecules, (Academic Press, New York, 1986), pp. 331-381.
5. P. Felenbok, Ann. Astrophys. **26**, 393 (1963).
6. I. Easson and M. H. L. Pryce, Can. J. Phys., **51**, 518 (1973).